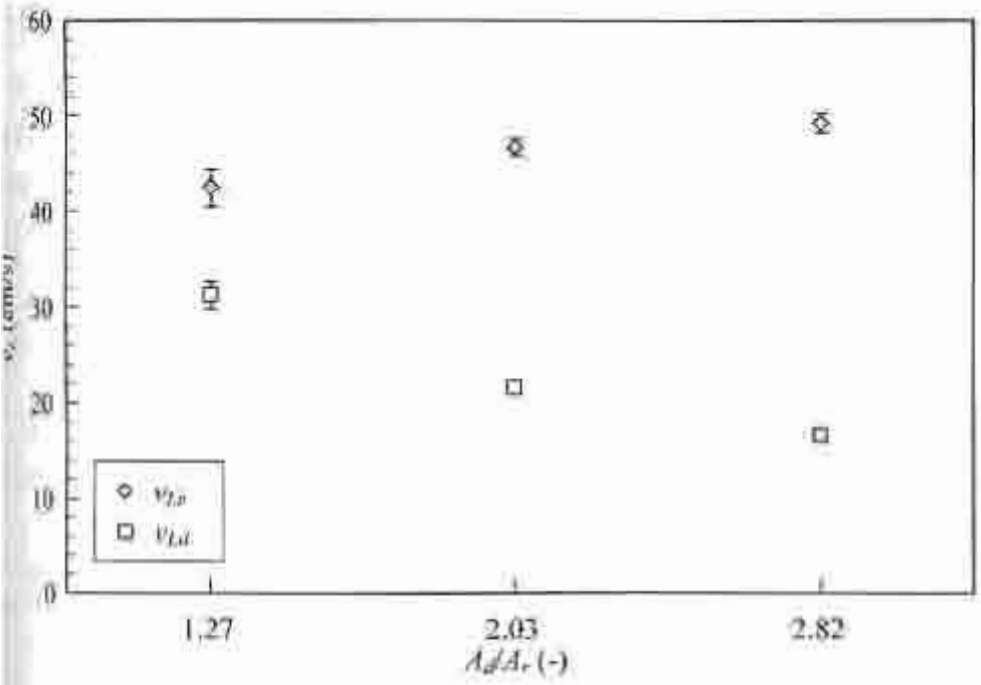

Fig. 7. Effect of A_d/A_r on liquid velocities (SW30, u_{sg}=2 cm/s).

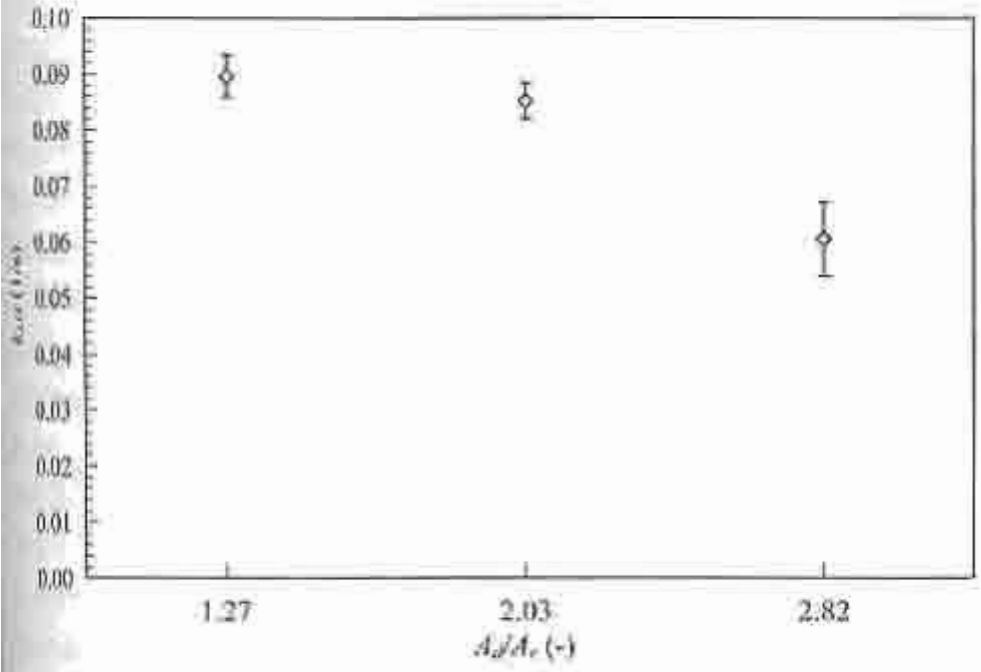

Fig. 8. Effect of A_d/A_r on overall volumetric mass transfer coefficient (SW30, u_{sg}=2 cm/s).

nomenon occurred. As the gas flowed more uniformly in the riser of such system, liquid moved at a lower speed. The re-circulating liquid then entered the downcomer, which in this case, had a smaller area size. Therefore, high downcomer liquid velocity was observed.

3-3. Effect of A_d/A_r on Overall Volumetric Mass Transfer Coefficient

An increase in A_d/A_r adversely affected the gas-liquid mass transfer rate as indicated in Fig. 8. This was not surprising as the airlift with large A_d/A_r was found to contain low gas holdup, which resulted in a small interfacial area between gas and liquid. Consequently, a low k_La was obtained as observed in ALC-5. On the other hand, ALC-3 allowed more bubbles to move into the downcomer, increasing the gas-liquid mass transfer area, and therefore a higher level of k_La was acquired. Although an airlift with a lower A_d/A_r tended to have a greater k_La than the system with a large A_d/A_r, it should be noted that the behavior of such system would approach that of the bubble column, i.e., a low riser liquid velocity and the existence of internal recirculation inside the draft tube could be well observed. A low liquid velocity would imply a higher chance of solid settlement, which could be detrimental for some applications involving three phases such as cell cultivation systems. In such case, a large A_d/A_r airlift system could then be useful as the appearance of a stronger liquid velocity could partially support the gas-liquid-solid mixing.

3. Influence of Salinity on Airlift Contactor Performance

The airlift system using a mixture of tap water and seawater at salinity of 15, 30, 45 ppt was compared. All experiments were performed in the airlift contactor with four 20 cm i.d. internal draft tubes where A_d/A_r was fixed at 2.03 (ALC-4). In the following discussion, "SW" is defined as seawater and the number following "SW" indicates the level of salinity in the unit of ppt, e.g., SW15=seawater at salinity of 15 ppt.

3-1. Effect of Salinity on Gas Holdups

Gas holdup in the airlift contactor was demonstrated to be influenced significantly by salinity levels. Fig. 9 illustrates that the system running with fresh tap water always had the lowest gas holdups. As the salinity increased, higher gas holdup was observed. However, the effect of salinity was only pronounced at high gas throughput condition (u_{sg}>1 cm/s).

It is known that salinity changed physical properties of the liquid by raising its surface tension, viscosity and density, and this strongly affected bubble size in the system [Prince and Blanch, 1990; Al-Masry, 1999]. High surface tension at high salinity level indicated stronger bubble surface force, which inhibited bubble coalescence. Hence, in the system with fresh tap water (low surface tension),

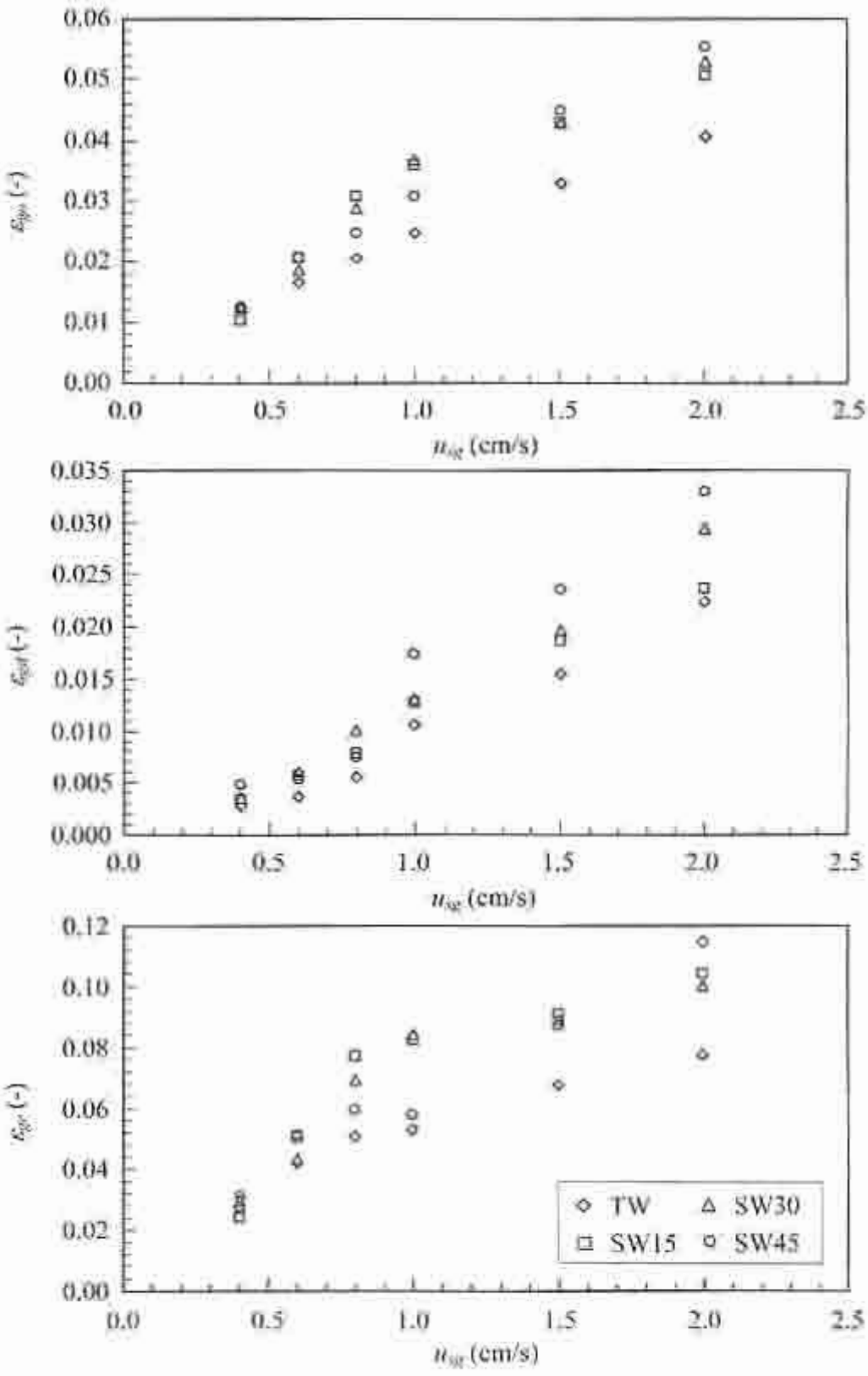

Fig. 9. Effect of salinity on gas holdups (ALC-4).

coalescence seemed to take place more intensively as a result of bubble-bubble interaction. This resulted in a larger bubble size. Large bubbles moved upwards rapidly due to high buoyancy force and caused a poor recirculation of bubbles within the system. This loss of bubbles reduced the total gas volume in the liquid resulting in low gas holdup.

The overall gas holdup in the airlift contactors operating at the various levels of salinity was found to increase with salinity level. Experiments revealed that the system with SW45 accommodated slightly higher gas holdup than the systems with SW30 and SW15, respectively, particularly at high gas throughput. This might be due to the existence of tiny bubble size in SW45, which facilitated the inducement of gas bubbles into the downcomer causing more bubbles to be recirculated within the system. Note that it was difficult to distinguish the sizes of bubbles obtained from the systems running with seawater at various salinity levels. Visual inspection alone could not identify the actual size with adequate accuracy. The system was also performed at a relatively high gas throughput, which was not suitable for measurement with a digital camera due to the bubble shading effects. The size of the bubbles inside the system was therefore estimated from observation.

3-2. Effect of Salinity on Liquid Velocity

Fig. 10 illustrates the effect of salinity on liquid velocities. It was observed that both riser and downcomer liquid velocities in the system with tap water were slightly higher than that obtained in the airlift with seawater. This was because the system with tap water was operated with larger bubbles which moved at a faster speed than smaller ones due to their high buoyancy force, and therefore induced through a momentum and energy transfer, a faster liquid movement. However, in this experiment, the difference in salinity levels (15, 30, and 45 ppt) was not found to have significant influence on liquid velocities.

3-3. Effect of Salinity on Overall Volumetric Mass Transfer Coefficient

The overall volumetric mass transfer coefficient, k_La, was clearly shown to be superior in the system operated with high salinity seawater rather than at low salinity (Fig. 11). Previous discussion demonstrated that liquid velocity was not significantly affected by the salinity. Therefore, it was expected that k_La would only be influenced by the changes in bubble characteristics which were altered as a result of changes in salinity. At high salinity, bubble size became small and this increased the interfacial area between gas and liquid. This meant that the specific surface area, "a," increased with salinity. In fact, "k_L" was regulated by the difference between liquid and bubble velocities, and therefore the bubble size would also have effects on this parameter. In other words, larger bubbles would move at faster speed, and as the liquid velocity did not change with salinity, the system with larger bubbles would have had a larger difference in bubble and liquid velocities, resulting in a high "k_L". This meant that the airlift system would have higher "a" but lower "k_L" at high salinity level than at low salinity. As the apparent k_La was a consequence of these two effects, higher k_La as a result of increasing salinity suggested that the effect of salinity on "a" could be more significant than that on "k_L".

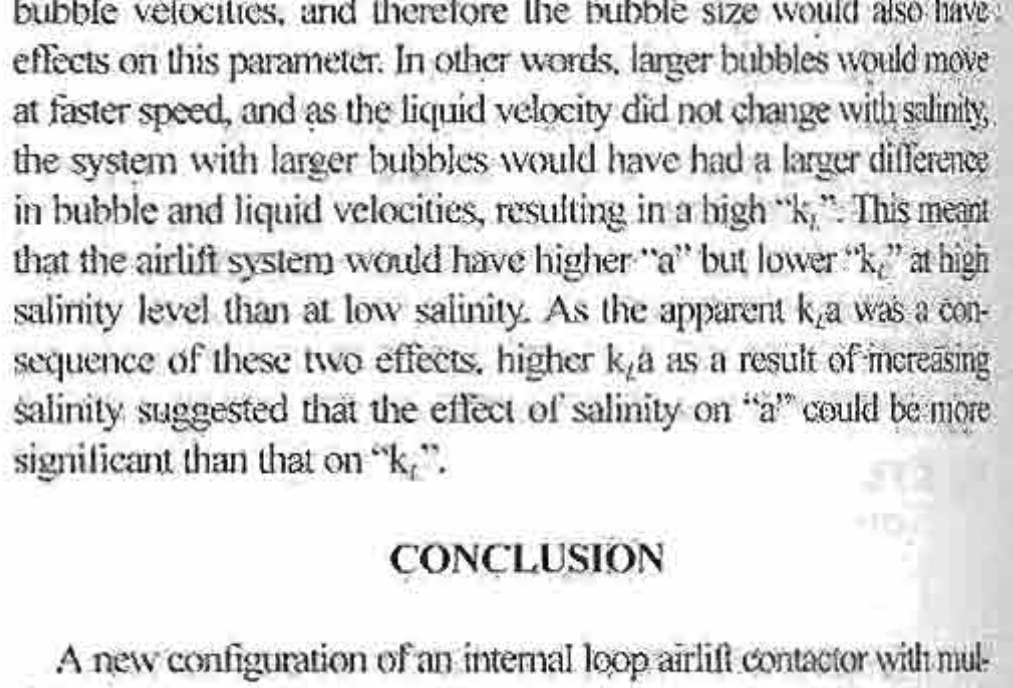

Fig. 11. Effect of salinity on overall volumetric mass transfer coefficient (ALC-4, u_g=2 cm/s).

CONCLUSION

A new configuration of an internal loop airlift contactor with multiple draft tubes was proposed in this work. The hydrodynamics and mass transfer in a large-scale operation of the proposed configuration were observed at different u_g, A_d/A_r and salinity levels and compared with a conventional single draft tube system. Increasing the number of draft tubes enhanced the connecting area between riser and downcomer leading to a better recirculation of fluid inside the airlift system. This also resulted in a higher gas-liquid interfacial area essential for mass transfer. Hence, the multiple draft tube

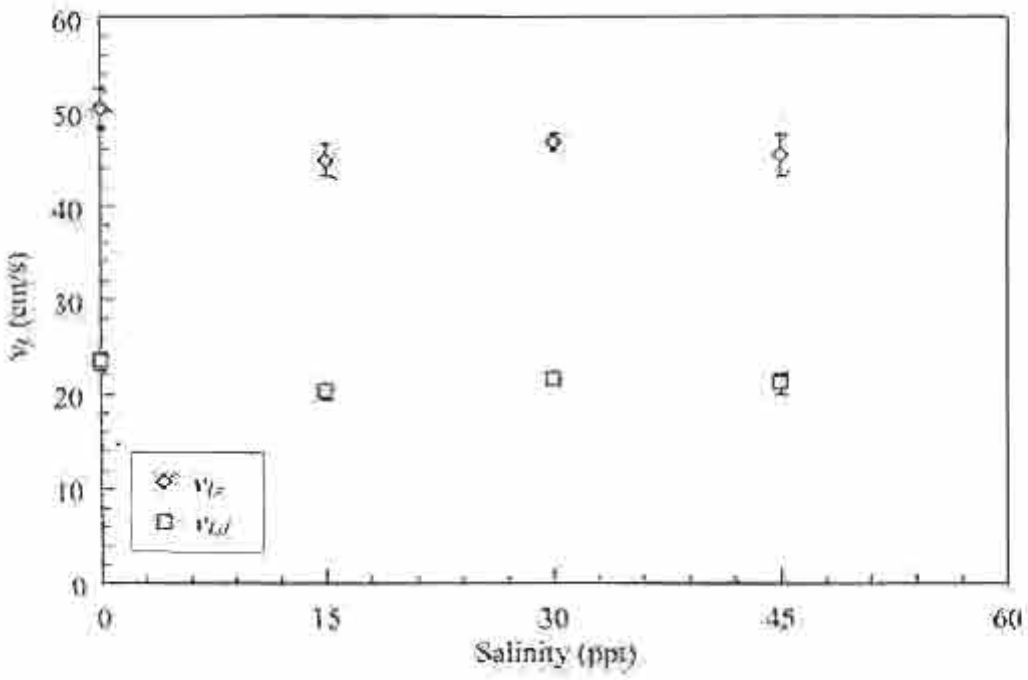

Fig. 10. Effect of salinity on liquid velocities (ALC-4, u_g=2 cm/s).

Table 2. Empirical correlations for overall volumetric mass transfer coefficient

	k_La (1/s)	Salinity (ppt)	R^2
ALC-1	$k_La=0.0251u_g^{0.81}$	30	0.9815
ALC-2	$k_La=0.0363u_g^{0.99}$	30	0.9669
ALC-3	$k_La=0.0556u_g^{0.77}$	30	0.9894
ALC-4	$k_La=0.0495u_g^{0.89}$	30	0.9872
ALC-5	$k_La=0.0277u_g^{1.03}$	30	0.9793
ALC-4	$k_La=0.0175u_g^{0.77}$	0	0.9717
ALC-4	$k_La=0.0438u_g^{0.97}$	15	0.9861
ALC-4	$k_La=0.0600u_g^{0.88}$	45	0.9784

airlift contactor was proven to be a potential system for the large-scale operation, especially in the case where a very large cross-sectional area is required. In this investigation, the overall volumetric mass transfer coefficients could be estimated relatively accurately by using the empirical correlations as proposed in Table 2.

ACKNOWLEDGMENTS

The authors wish to acknowledge the Thailand Research Fund for their financial support.

NOMENCLATURE

A_d : downcomer cross-sectional area [m^2]
a : specific gas-liquid interfacial area [m^2/m^3]
A_r : riser cross-sectional area [m^2]
D_{DT} : draft tube diameter [m]
k_L : mass transfer coefficient [m/s]
k_La : overall volumetric mass transfer coefficient [1/s]
N_{DT} : number of draft tube
u_g : superficial gas velocity [cm/s]
v_L : liquid velocity [cm/s]

Abbreviation

ALC : airlift contactor
ppt : part per thousand
SW : seawater
TW : tap water

Greek Letters

ε_{gd} : downcomer gas holdup [-]
ε_g : overall gas holdup [-]
ε_{gr} : riser gas holdup [-]

Subscripts

d : downcomer
r : riser

REFERENCES

Al-Masry, W. A., "Effects of antifoam and scale-up on operation of bioreactors," *Chem. Eng. Process*, **38**, 197 (1999).

Blažej, M., Kiša, M. and Markoš, J., "Scale influence on the hydrodynamics of an internal loop airlift reactor," *Chem. Eng. Process*, **43**, 1519 (2004).

Camacho, F. G., Grima, E. M., Mirón, A. S., Pascual, V. G and Chisti, Y., "Carboxymethyl cellulose protects algal cells against hydrodynamic stress," *Enzyme and Microbial Technology*, **29**, 602 (2001).

Choi, K. H., Chisti, Y. and Moo-Young, M., "Comparative evaluation of hydrodynamic and gas-liquid mass transfer characteristics in bubble column and airlift slurry reactors," *Chem. Eng. J.*, **62**, 223 (1996).

Gopal, J. S. and Sharma, M. M., "Hydrodynamic and mass transfer characteristics of bubble and packed bubble columns with downcomer," *Can. J. Chem. Eng.*, **60**, 353 (1982).

Heijnen, J. J., Hols, J., van der Lans, R. G J. M., van Leeuwen, H. L. J. M., Mulder, A. and Weltevrede, R., "A simple hydrodynamic model for the liquid circulation velocity in a full-scale two- and three-phase internal airlift reactor operating in the gas recirculation regime," *Chem. Eng. Sci.*, **52**(15), 2527 (1997).

Jianping, W., Xiaoqiang, J., Lei, P., Changlin, W. and Guozhu, M., "Nitrifying treatment of waste water from fertilizer production in a multiple airlift loop bioreactor," *Biochem. Eng. J.*, **25**, 33 (2005).

Koide, K., Iwamoto, S., Takasaka, Y., Matsuura, S., Takahashi, E. and Kimura, M., "Liquid circulation, gas holdup and pressure drop in bubble column with draught tube," *J. Chem. Eng. Jpn.*, **17**(6), 611 (1984).

Krichnavaruk, S., Loataweesup, W., Powtongsook, S. and Pavasant, P., "Optimal growth conditions and the cultivation of Chaetoceros calcitrans in airlift photobioreactor," *Chem. Eng. J.*, **105**, 91 (2005).

Merchuk, J. C., Ladwa, N., Cameron, A., Bulmer, M. and Pickett, A., "Concentric-tube airlift reactors: effects of geometrical design on performance," *AIChE J.*, **40**(7), 1105 (1994).

Mirón, A. S., Garć, M. C. C., Gómez, A. C., Camacho, F. G., Grima, E. M. and Chisti, Y., "Shear stress tolerance and biochemical characterization of *Phaeodactylum tricornutum* in quasi steady-state continuous culture in outdoor photobioreactors," *Biochem. Eng. J.*, **16**, 287 (2003).

Prince, M. J. and Blanch, H. W., "Transition electrolyte concentrations for bubble coalescence," *AIChE J.*, **36**(9), 1425 (1990).

Russell, A. B., Thomas, C. R. and Lilly, M. D., "The influence of vessel height and top-section size on the hydrodynamic characteristics of airlift fermentors," *Biotech. Bioeng.*, **43**, 69 (1994).

Shamlou, P. A., Pollard, D. J. and Ison, A. P., "Volumetric mass transfer coefficient in concentric-tube airlift bioreactors," *Chem. Eng. Sci.*, **50**(10), 1579 (1995).

Silapakul, S., Powtongsook, S. and Pavasant, P., "Nitrogen compounds removal in a packed bed external loop airlift bioreactor," *Korean J. Chem. Eng.*, **22**, 393 (2005).

Wongsuchoto, P. and Pavasant, P., "Internal liquid circulation in annulus sparged internal loop airlift contactors," *Chem. Eng. J.*, **100**, 1 (2004).

ภาคผนวก 3

"Photoautotrophic High-Density Cultivation of Vegetative Cells of *Haematococcus pluvislis* in Airlift Bioreactor" K. Kaewpintong, A. Shotipruk, S. Powtongsook and P. Pavasant, Bioresource Technology 98 (2007), 288-298

Available online at www.sciencedirect.com
ScienceDirect
Bioresource Technology 98 (2007) 288–295
BIORESOURCE TECHNOLOGY

Photoautotrophic high-density cultivation of vegetative cells of *Haematococcus pluvialis* in airlift bioreactor

Kamonpan Kaewpintong [a], Artiwan Shotipruk [a], Sorawit Powtongsook [b], Prasert Pavasant [a,*]

[a] *Department of Chemical Engineering, Faculty of Engineering, Chulalongkorn University, Bangkok 10330, Thailand*
[b] *Marine Biotechnology Research Unit (at Chulalongkorn University), National Center of Genetic Engineering and Biotechnology, Bangkok 10330, Thailand*

Received 12 September 2005; received in revised form 12 January 2006; accepted 17 January 2006
Available online 3 March 2006

Abstract

This work aimed to investigate the effects of the bioreactor configurations and their design variables on the cultivation of vegetative cells *Haematococcus pluvialis* to achieve sustainable high cell density. The addition of vitamin B to F1 growth medium could appreciably enhance the final cell density. Employing this medium, the cultivation in the airlift bioreactor was demonstrated to outperform the bubble column at the same operating conditions. Aeration was crucial for a proper growth of the alga in the airlift bioreactor, but it must be maintained at low level to minimize shear stress. The most appropriate aeration velocity (superficial velocity) was at the lower limit of the pump, i.e. 0.4 cm s^{-1} and a smaller riser was shown to have positive influence on the cell growth. A 1% CO_2 supplement to the air supply considerably enhanced the growth rate of *H. pluvialis* and the most suitable light intensity for the growth was at 20 μmol photon m^{-2} s^{-1}. The semi-continuous culture was successfully implemented with the optimal airlift bioreactor design and under optimal conditions the harvest could be performed every four days with the specific growth rate of 0.31 d^{-1}.

Keywords: Airlift bioreactors; Astaxanthin; Autotrophic; Bioprocess design; Bubble columns; Microalgae

1. Introduction

Astaxanthin or 3,3′-dihydroxy-β-β-carotene-4,4′-dione, a red ketocarotenoid, has currently gained much interest due to its versatile applications in aquacultural, food, pharmaceutical, and nutraceutical industries (Lorenz and Cysewski, 2000). The compound is widely employed as a pigmentation inducer, and due to its good biological function such as antioxidant activity, it has been used for immune response enhancement and cancer protection (Kobayashi et al., 1991). Astaxanthin can be extracted from natural sources or chemically synthesized. However, synthesized astaxanthin was reported to contain unnaturally configurational carotenoid compounds, which might not be as effective as that produced naturally (Gong and Chen, 1997; Johnson and An, 1991). As a result, tremendous interest has been placed on production of natural astaxanthin, which is generally found in microorganisms such as some yeast and microalgae.

Of all the astaxanthin accumulated microorganisms, the green alga, *Haematococcus pluvialis* has been reported to accumulate the highest amount of astaxanthin (Gong and Chen, 1997; Harker et al., 1996; Kobayashi et al., 1991). However, due to its slow growth, susceptibility to contamination, and preference for low growth temperature (Harker et al., 1996), outdoor cultivation of *H. pluvialis* has generally become unsuccessful. This leads to the need for the cultivation in closed systems, which offers a number of advantages including better control of culture environment, protection from ambient contamination and achievement of high cell density.

* Corresponding author. Tel.: +662 218 6870; fax: +662 218 6877.
E-mail address: prasert.p@chula.ac.th (P. Pavasant).

0960-8524/$ - see front matter © 2006 Elsevier Ltd. All rights reserved.
doi:10.1016/j.biortech.2006.01.011

Numerous studies have been conducted to investigate the cultivation of *H. pluvialis* in culture flasks under controlled environment (Tripathi et al., 2002; Grunewald et al., 1997; Sarada et al., 2002; Kobayashi et al., 1991, 1992). Hata et al. (2001) reported the highest maximum cell density of 100×10^4 cells mL^{-1} in a 500 mL flask. In practice, for large-scale production, *H. pluvialis* culture must be carried out in a bioreactor. Various types of bioreactors such as stirred tank, bubble column, and airlift bioreactor have been employed in several studies (Harker et al., 1996; Chen et al., 1997; Zhang et al., 1999). Among these, the highest cell density was achieved in a stirred tank reactor but it was only 29.4×10^4 cells mL^{-1} (Harker et al., 1996). For slow growth, shear sensitive cells (such as *H. pluvialis*), pneumatically agitated bioreactors are recommended over mechanically stirred reactors due to their design simplicity and low shear force. Examples of such pneumatic devices include bubble column and airlift bioreactor, which have lately been applied to a variety of biotechnological processes. These types of bioreactor have been employed for cultivation of *H. pluvialis*. For example, Choi et al. (2003) examined lumostatic operation of bubble columns for *H. pluvialis* culture, and Harker et al. (1996) studied the effect of NaCl addition on astaxanthin production in airlift bioreactors. However, their studies did not emphasize on the aspect of achieving high cell density and only 25×10^4 cells mL^{-1} was obtained. To the authors' knowledge, a study which focuses on the effects of the bioreactor configurations and their design variables on the culture growth of *H. pluvialis* is nonexistent. This work specifically aimed to investigate the cultivation of vegetative cells of *H. pluvialis* in airlift bioreactors to achieve sustainable high cell density and to determine the effect of various system variables on cell density and specific growth rate. As *H. pluvialis* is prone to easy contamination particularly in the presence of added organic carbon source, in this study, the cells were therefore grown photoautotrophically. Initial experiments were conducted to determine the most suitable growth medium and vitamin B concentration. The selected medium was then employed in the cultivation of the cells in the lab-scale bubble and airlift bioreactors to compare the performance of the two types of bioreactor. Cell cultivation in airlift bioreactor was then investigated to determine the optimal growth conditions. Finally, to examine the potential of implementing large-scale production, semicontinuous cultivation of *H. pluvialis* was conducted.

2. Methods

2.1. Microorganisms and inoculum preparation

H. pluvialis (NIES 144) was obtained from the National Institute of Environmental Studies culture collection,

Table 1
Composition of culture media examined in this work (all for one litre of medium)

	M1 [8]	Basal [11]	F1 [1]	BG-11 [12]	Hong Kong [10]	M6 [9]
$CaCl_2 \cdot 2H_2O$	183.8 mg	25 mg	9.78 mg	36 mg	73 mg	3.676 g
KNO_3	0.5 g	10 mg	0.41 g		0.3 g	
$NaNO_3$				1.5 g		
Na_2HPO_4			0.03 g		30 mg	1.5 g
NaH_2PO_4	195 mg				35.5 mg	1.778 g
H_3PO_4	0.12 mg					12.37 mg
K_2HPO_4		75 mg		40 mg		
KH_2PO_4		175 mg				
NaCl		2.513 g				
KOH		30.85 mg				
H_2SO_4		0.99 mg				
$C_6H_5FeO_7 \cdot 5H_2O$			2.21 mg			
$FeSO_4 \cdot 7H_2O$	20.9 mg	4.976 mg			8.3 mg	0.417 g
$MgSO_4 \cdot 7H_2O$	61.6 mg	4 mg	16.41 mg	75 mg	24.6 mg	1.231 g
$ZnSO_4$	0.72 mg	8.827 μg			0.014 mg	71.89 mg
$CuSO_4 \cdot 5H_2O$	0.62 mg	1.572 g	0.008 mg	0.079 mg	0.012 mg	62.42 mg
$Na_2MoO_4 \cdot 2H_2O$	0.07 mg		0.08 mg	0.39 mg	0.001 mg	7.26 mg
$CoCl_2 \cdot 2H_2O$	0.05 mg		0.0078 mg		0.0005 mg	4.67 mg
H_3BO_3		10.948 mg		2.86 mg	0.003 mg	
Cr_2O_3			0.05 mg			
SeO_2			0.036 mg			
$EDTANa \cdot 2H_2O$	18.6 g	49.34 mg		1 mg	6.7 mg	0.372 g
Na_2CO_3				0.02 g		
$NH_4Fe(C_6H_5O_7)$				0.006 g		
$MnCl_2 \cdot 4H_2O$		1.445 mg	0.66 mg	1.81 mg		
$ZnSO_4 \cdot 7H_2O$				0.222 mg		
$Co(NO_3)_2 \cdot 6H_2O$		0.389 mg		0.049 mg		
$MnSO_4 \cdot H_2O$	0.72 mg				0.001 mg	84.51 mg
$Ca(NO_3)_2 \cdot 4H_2O$		15 mg				

Japan. *H. pluvialis* was initially cultivated in the standard sterilized F1 medium (Fábregas et al., 1998) in a 250 mL flask at 27 ± 1 °C with a continuous illumination of white fluorescent light at the intensity of 20 μmol photon m^{-2} s^{-1}. This culture was then up-scaled to 600 mL before transferring to the bioreactor. Only the green motile cells from exponential growth phase were used as inoculums for all experiments.

2.2. Culture media experiments

To test the effect of culture media, all culture experiments were conducted in 250 mL flasks with 10% inoculum volume. The culture condition was again controlled at 27 ± 1 °C with a continuous illumination of 20 μmol photon m^{-2} s^{-1} by fluorescent lights. Seven previously reported culture media for the autotrophic growth of *H. pluvialis* were tested, including: M1 (Chen et al., 1997), M6 (Gong and Chen, 1998), F1 (Fábregas et al., 1998), Hong Kong (Zhang et al., 1999), Basal (Hata et al., 2001), BG-11 (Boussiba and Vonshak, 1991), and Basal:BG-11 (1:1). The compositions of each culture medium were summarized in Table 1. In addition, the effect of vitamin B complex was determined using the most suitable type of medium. The vitamin B complex was commercially available with the ratio between B1, B6, and B12 of 1.33:0.1:1. In the discussion hereafter the quantity of vitamin B complex will be referred to using the vitamin B12 content. The range of the vitamin investigated in this work was between 0.5 and 20 μg L^{-1}.

2.3. Bioreactor setup

Both bubble column and airlift bioreactors were made of a clear acrylic plastic. The schematic diagrams along with the dimensions of the two systems are shown in Fig. 1. The airlift bioreactor was simply the bubble column with a draft tube that was centrally installed within the outer column. Prior to each experiment, the bioreactors were sterilized by sparging ozone through the 0.45 μm Gelman autoclavable filter and a flow meter into the water at the base of the bioreactor for 1 h. Ozone was subsequently substituted by compressed air for another 3–4 h to remove ozone residual. The bioreactor was then filled with 3000 mL of culture with approximately 250 mL of starter innoculum. This accounted for an initial density of *H. pluvialis* of 2×10^4 cells mL^{-1}. Mixing in the bioreactor was obtained by introducing compressed air at the base of the bioreactor through the porous sparger. The media prepared as described had an initial pH of 7.1. In the experiment with an addition of CO_2, compressed air, and CO_2 gas were mixed and metered through calibrated flow meters before entering the system. The concentration of CO_2 used in this study was lower than 2% v/v, which was found not to affect the pH significantly as CO_2 was continuously taken up by the algae during the course of cultivation. In

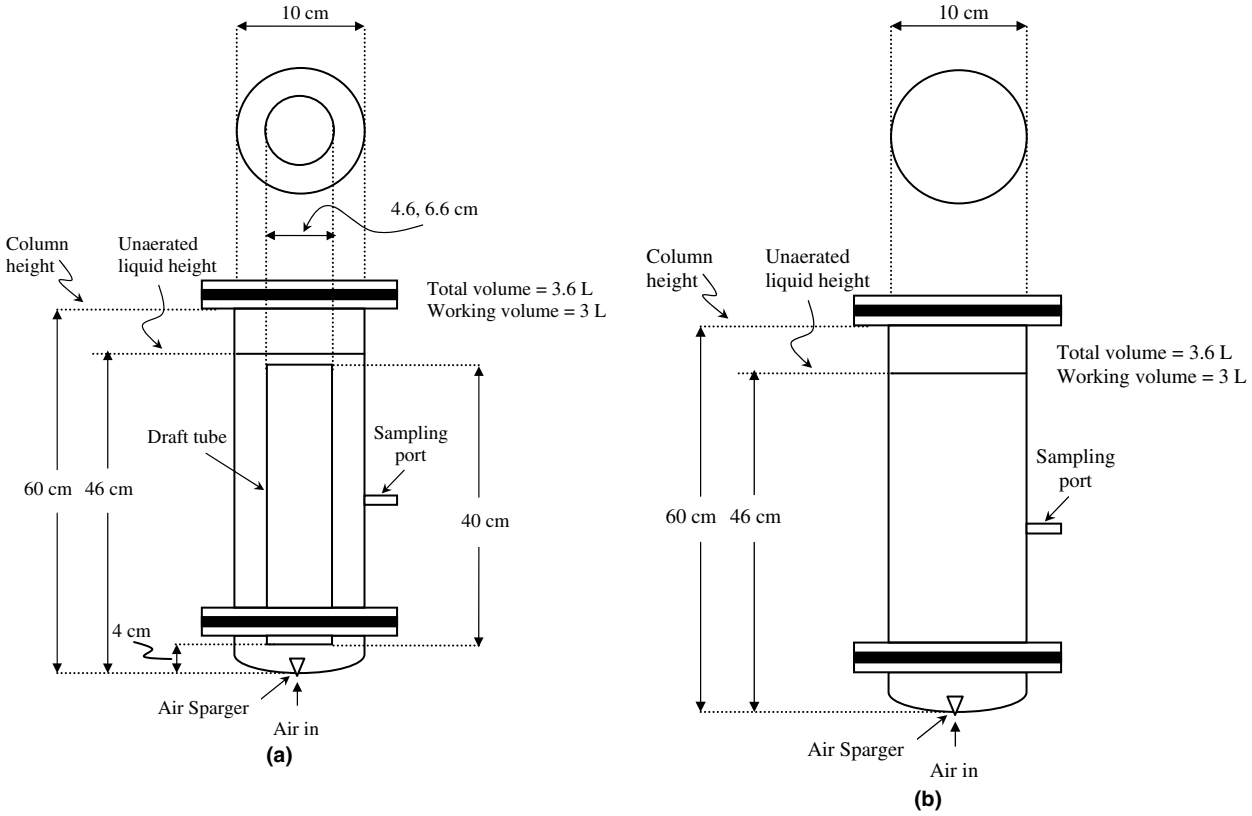

Fig. 1. Schematic diagrams of (a) airlift bioreactor and (b) bubble column, employed in this work.

this system, the temperature was controlled in the range of 27 ± 1 °C. Light was supplied to the bioreactor from the 18 W fluorescent lamps installed vertically along the length of the column. The distance between the lamps and the column was set at 3 cm. The illumination intensity was adjusted by altering the number of lamps and the distance between the lamps and the surface of the bioreactor. The average illumination intensity incident to the bioreactor outer surface was measured with a digital lux meter (DIGICON LX-50).

2.4. Determination of suitable operating conditions

Experiments were carried out to determine the effect of different factors on the cell growth including the type of reactors, i.e. airlift and bubble column, the concentration of CO_2, the superficial gas velocity, the ratio between the downcomer and riser cross sectional area, and illumination intensity. All experiments were carried out in triplicate. In the batch operation, the culture was grown in the bioreactor until the stationary phase was reached, whereas in the semi-continuous mode, the cultivation was started out as a batch culture, where a 50% by volume of culture broth during the exponential growth phase was replaced with a fresh medium. The algal cell density was measured daily by microscope counting using an improved Neubauer haemacytometer. From the cell density, specific growth rate (μ; d^{-1}) was calculated from

$$\mu = \frac{\ln(N_2/N_1)}{t_2 - t_1}, \quad (1)$$

where N_1 and N_2 (cells mL^{-1}) are cells densities at time t_1 and t_2 (d). The cell productivity (cells mL^{-1} d^{-1}) was calculated from

$$\text{Productivity} = \frac{C_2 - C_1}{t_2 - t_1}, \quad (2)$$

where C_1 and C_2 are cell densities at t_1 and t_2.

3. Results and discussion

3.1. Effect of the type of medium

The maximum cell density and specific growth rate obtained from different culture media are shown in Fig. 2. Interestingly, it was observed that the growth of *H. pluvialis* was greatly influenced by the type of culture medium. The growth was worst in M1 and M6 media and best in F1 in which the attained maximum cell density was 5.44×10^4 cells mL^{-1}. The growth in Basal:BG-11 medium was comparable to that in BG-11 alone. Hong Kong medium also resulted in similar growth characteristics with Basal:BG-11 and BG-11 media. For most of the cultures, cysts were observed when growth entered stationary phase (results not shown). This meant that some cells became inactive and no further cell division was expected. Although the cells started to lose their flagella as they converted to cysts, no accumulation of astaxanthin was apparent in M1, F1, and Hong Kong media even after 13 days of cultivation. This implied that cells could still sustain in these media but were not quite as active as the vegetative cells. With these findings, F1 medium was selected as the most suitable medium for subsequent experiments.

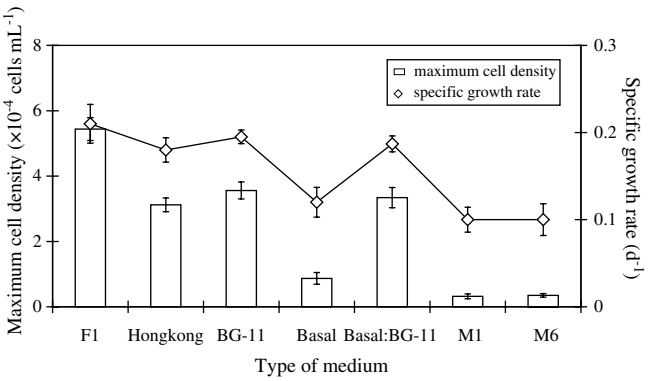

Fig. 2. Maximum cell density and specific growth rate *H. pluvialis* obtained from the cultivation in various types of medium.

The dependency of the specific growth rate on the various media was similar to that of the maximum cell concentration. As cells entered stationary phase at approximately the same time (day 8), the medium that provided the highest growth also gave the highest specific growth rate. In this experiment, F1 medium gave the highest growth rate of 0.21 d^{-1}. This was approximately at the same level as that reported by Tjahjono et al. (1994) who achieved the maximum specific growth rate of about 0.25 d^{-1} using Basal growth medium grown in mixotrophic condition with sodium acetate as a carbon source. However, this level was only about one third of the maximum reported value at 0.58 d^{-1}, which was the cultivation in the flask with Basal as growth medium growing in mixotrophic condition with sodium acetate as a carbon source (Kobayashi et al., 1992).

3.2. Effect of vitamin B concentration

Vitamin B has been often reported to have significant effects on the growth of microalgae. For example, thiamine (vitamin B1) was considered as a growth factor for microalgae, or vitamin B12 was employed to stimulate growth but was not essential (Pringsheim, 1996), etc. However, the reported findings on the significance of vitamin B for the cultivation of *H. pluvialis* were still not clear. Whilst Fábregas et al. (1998) found that *H. pluvialis* required thiamine together with vitamin B12 and biotin in order to achieve maximum growth (in F1 medium), Gong and Chen (1997) stated that vitamin B (including thiamine and vitamin B12) and also biotin had no significant effects on the growth rate of *H. pluvialis* (with M6 growth medium). In the seven types of medium examined above, vitamins had not been included. The objective here was therefore to demonstrate the effect of the addition of vitamin B on the growth of *H. pluvialis*.

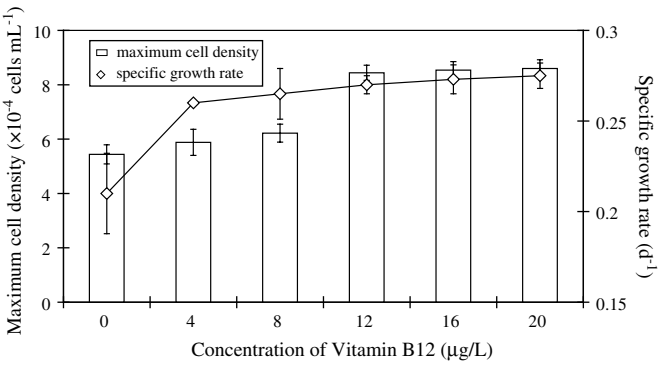

Fig. 3. Effect of vitamin B12 on maximum cell density and specific growth rate of *H. pluvialis*.

The growth curves from the cultivation of *H. pluvialis* in F1 medium with varying concentrations of vitamin B (referred to as the concentration of vitamin B12) are shown in Fig. 3. The cell density increased with the concentration of vitamin B12 up to 20 μg L^{-1}. The effect of vitamin B was more obvious at a low concentration range (4–12 μg L^{-1}), whereas only slight influence was observed above 12 μg L^{-1}. Therefore, vitamin B at 12 μg L^{-1} (of vitamin B12) was considered as an optimal level for the growth of *H. pluvialis* with F1 medium. At this vitamin concentration, the maximum cell density increased by approximately 55% when compared with cell growth in the medium without the addition of the vitamin. Although the effect of vitamin B on the specific growth rate of *H. pluvialis* was not as obvious as that on the maximum cell concentration, a 28.6% increase in the specific growth rate was observed as the vitamin level increased from 4 to 12 μg L^{-1}. Further increase in the vitamin concentration above 12 μg L^{-1} no longer led to significantly enhanced growth.

3.3. Comparison of growth in bubble column and airlift bioreactor

As *H. pluvialis* is highly sensitive to shear stress, reactors that induce high shear such as the commonly known stirred tanks are not recommended. Fortunately, *H. pluvialis* is a slow growth culture, which does not require a high rate of mass transfer and mixing, therefore, the use of high performance but energy intensive stirred tanks is not necessary. Pneumatic bioreactors, hence, emerge as an ideal alternative for such microorganism. In pneumatic systems such as bubble columns or airlift bioreactors, the mixing and mass transfer are induced just by the aeration, which generates very low level of shear and also is much less energy intensive than stirred tanks.

The comparison between the performances both bubble column and airlift bioreactor at $u_{sg} = 0.4$ cm s^{-1} at the same operating condition showed that the maximum cell density and of specific growth rate *H. pluvialis* grown in airlift bioreactor were 79.5×10^4 cells mL^{-1} and 0.45 d^{-1}, which were higher than those in bubble column which were 42×10^4 cells mL^{-1} and 0.36 d^{-1}, respectively. The similar findings were obtained at the other level of u_{sg} but the results were not shown here. The configuration in the airlift bioreactor provided a well defined flow pattern compared with the random flow pattern in the bubble column (Merchuk et al., 1998). Therefore most cells in the airlift system would circulate along the axial direction of the reactor and would be exposed to light, which was supplied along the reactor length. In other words, the uniform flow pattern in airlift bioreactor led to a certain movement of cells from dark (riser) to light (downcomer) zones. In the bubble column, on the other hand, no clear flow pattern was induced and therefore the movement of the cells inside the reactor was random, i.e. cells may have stayed at the regions with high or low light intensities for a long time without being recirculated. As cells were better exposed to light in the airlift bioreactor than in the bubble column, it was anticipated that photosynthesis took place more significantly in the airlift system. Therefore a better cell growth was observed in the airlift system than in the bubble column. In addition, visual inspection always suggested that there were a number of cell agglomerations, which resulted in the sedimentation of cells in the bubble column, the condition which was not found in the airlift bioreactor. Changes in morphology of alga from motile to non-motile were already observed in the bubble column even at the low level of aeration rate, which indicated that the condition in the bubble column might not be suitable for the algal growth.

3.4. Effect of CO_2

Chemical analysis showed that algal biomass consisted of approximately 40–50 wt% of carbon (Fischer and Alfermann, 1995). Hence, growth rate of photoautotrophic cultures essentially depends on a sufficient supply of carbon substrate for photosynthesis. In this work, *H. pluvialis* was grown in photoautotrophic condition with CO_2 as the main carbon source. Fig. 4 demonstrated that the addition of 1% by volume of CO_2 into the air stream supplied to the system resulted in the best cultivation performance both in terms of maximum cell density and specific growth rate. The

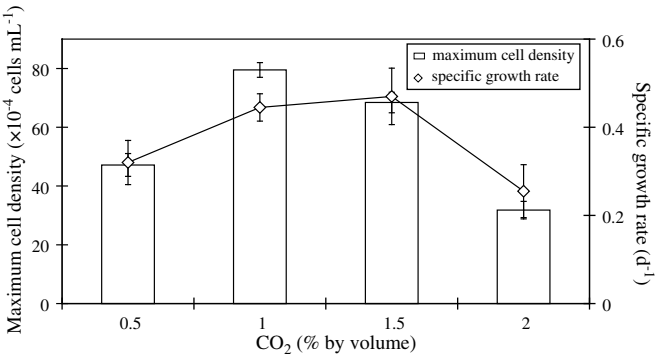

Fig. 4. Effect of CO_2 concentrations on maximum cell density and specific growth rate of *H. pluvialis* at $u_{sg} = 0.4$ cm s^{-1}.

attainable maximum cell density of 79.5×10^4 cells mL^{-1} or 2.79 g L^{-1} dry weight was equivalent to an almost 9.5 fold increase from the level obtained without the addition of CO_2. The specific growth rate for the system at 1% CO_2 was found to be 0.45 d^{-1}, which was considerably higher than the level obtained without CO_2 supplement. This clearly showed the importance of CO_2 for the cultivation of *H. pluvialis*, and subsequent experiments were performed using the air stream with the addition of 1% CO_2.

3.5. Effect of superficial velocity

To study the effect of aeration rate on the cell growth, experiments were conducted in the airlift system ($A_d/A_r = 3.2$) operating with different levels of aeration rate in the range of 0.4–3 cm s^{-1} (as measured in terms of superficial velocity, u_{sg}). When the column was not aerated, there was only a slight increase in cell concentration from the initial level of 2×10^4 cells mL^{-1} to 3.59×10^4 cells mL^{-1} (0.08 g L^{-1} dry weight) after 10 days of cultivation (results not shown). The highest growth of *H. pluvialis* was resulted at u_{sg} of 0.4 cm s^{-1}, with the maximum cell density and maximum specific growth rate of 79.5×10^4 cells mL^{-1} and 0.45 d^{-1}, respectively. Interestingly however, further increase in the aeration rate (above the superficial gas velocity of 0.4 cm s^{-1}) did not show benefits for the growth. In fact, for the higher flow velocities of 2, 2.5, and 3 cm s^{-1}, the maximum cell density decreased drastically to 26×10^4, 9×10^5, and 6×10^4 cells mL^{-1}, and the specific growth rate to 0.34, 0.32, and 0.11 d^{-1}, respectively. Due to the equipment constraints, the air-flow could not be accurately adjusted below 0.4 cm s^{-1}, therefore it could not be concluded at this point that this 0.4 cm s^{-1} of superficial gas velocity was the optimal level. However, the specific growth rate obtained at this condition (0.45 d^{-1}) was significantly higher than most of the reported data in the literature, and was only second to Kobayashi et al. (1992) who achieved the specific growth rate of 0.58 d^{-1} with the 100 mL culture growing in mixotrophic condition.

Increasing aeration rate generally induces mixing, liquid circulation, and mass transfer between gas and liquid phases in the airlift systems (Krichnavaruk and Pavasant, 2002). A higher mass transfer might also facilitate the removal of gases such as oxygen, preventing the accumulation, which might cause adverse effect on the growth (Tung et al., 1998). However, the cell culture of *H. pluvialis* in the batch culture in the airlift system was negatively affected by an increase in superficial gas velocity over 0.4 cm s^{-1}. This was believed to be due to the shear stress caused by the high aeration rate. This indicated that the cell of *H. pluvialis* was highly shear sensitive and even the shear caused by aeration could deteriorate the growth. This explanation was supported by several past reports. For instance, Gudin and Chaumont (1991) stated that the key problem in the cultivation of microalgae in photobioreactors was cell damage due to shear stress. Hata et al. (2001) illustrated

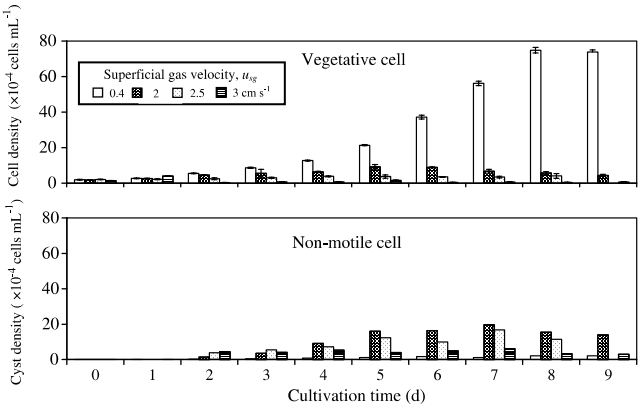

Fig. 5. Density of vegetative cells and cysts of *H. pluvialis* obtained from operation at various u_{sg}.

that the culture of green vegetative cell in exponential phase of growth required a low liquid velocity due to its fragility. To further examine the effect of the aeration, the structure of *H. pluvialis* under various aeration rates was monitored. The results as summarized in Fig. 5, illustrated that an increase in superficial gas velocity could significantly change the cell morphology from vegetative cells to non-motile green cells or cysts. In other words, the fraction of non-motile cells became more dominant with an increase in the aeration rate. At the superficial velocity of 0.4 cm s^{-1}, a very small fraction of non-motile green cells was observed when compared to the number of vegetative cells. On the other hand, the number of vegetative cells could hardly be observed at the superficial velocity greater than 2.5 cm s^{-1}. The vegetative cells are more productive in view of cell multiplication, and it would be difficult to obtain high cell density if the cell could not be maintained in vegetative form particularly in high shear stress condition.

3.6. Effect of the ratio between downcomer and riser cross sectional area

This section examined the effect of design configuration of the airlift system, i.e. the ratio between downcomer and riser cross sectional area (A_d/A_r) on the growth of *H. pluvialis*. This parameter could be simply altered by changing the draft tube size. Due to a size constraint, a rather smaller airlift column could only accommodate two sizes of commercially available clear column (employed as draft tube), i.e. at 4.6 and 6.6 cm. This gave A_d/A_r of approximately 3.2 and 0.9, respectively.

The result demonstrated that the airlift with A_d/A_r of 3.2 could deliver a significantly higher level of growth. The maximum cell density and specific growth rate were 79.5×10^4 cells mL^{-1} and 0.45 d^{-1} for A_d/A_r of 3.2, whereas the values were 46×10^4 cells mL^{-1} and 0.38 d^{-1} for A_d/A_r of 0.9. A higher A_d/A_r meant that the system was equipped with a smaller riser, and this enhanced the riser liquid velocity whilst considerably decreased the downcomer liquid

velocity (as downcomer had a much greater cross sectional area than riser). As the light was only supplied on the outer surface of the column, cells in downcomer were better exposed to light than those in riser. Therefore, the low downcomer liquid velocity possibly allowed cells in this section to utilize light for a longer time period and this seemed to have positive influence on the cell growth.

3.7. Effect of light intensity

The experiment with light intensity was carried out in the batch cultivation mode using the airlift bioreactor with A_d/A_r of 3.2 and u_{sg} of 0.4 cm s^{-1}. Five different surface light intensities were tested and the results on growth profiles and the maximum cell density are shown in Fig. 6.

The results revealed that the cell density and specific growth rate increased with an increase in the light intensity up to 20 μmol photon m^{-2} s^{-1}. Further increase in light intensity, on the other hand, resulted in lower cell density and specific growth rate, which could have indicated the occurrence of photoinhibition. Fig. 7 illustrated that at light intensity lower than 40 μmol photon m^{-2} s^{-1}, almost all the cells were in vegetative form. The light intensity over 50 μmol photon m^{-2} s^{-1} was likely to induce morphological change, i.e. cells changed from vegetative cells to cysts, with a concomitant accumulation of astaxanthin. This emphasized the fact that astaxanthin accumulation in *H. pluvialis* could be induced at high light intensity. Similar finding was observed previously by Boussiba and Vonshak (1991), which showed that an accumulation of astaxanthin was stimulated with a light intensity of over 90 μmol photon m^{-2} s^{-1}. However, the results here demonstrated that astaxanthin could well be accumulated at the light intensity of as low as 40 μmol photon m^{-2} s^{-1}. Moreover, cell growth was no longer observed when the light intensity increased to 60 μmol photon m^{-2} s^{-1}.

In terms of growth, the accumulation of astaxanthin was not a good sign as this was the condition where cell division began to cease. Therefore, this condition must be avoided should the growth be the main objective of the cultivation. Hence, the optimal light intensity for the growth of *H. pluvialis* was concluded to be at 20 μmol photon m^{-2} s^{-1}.

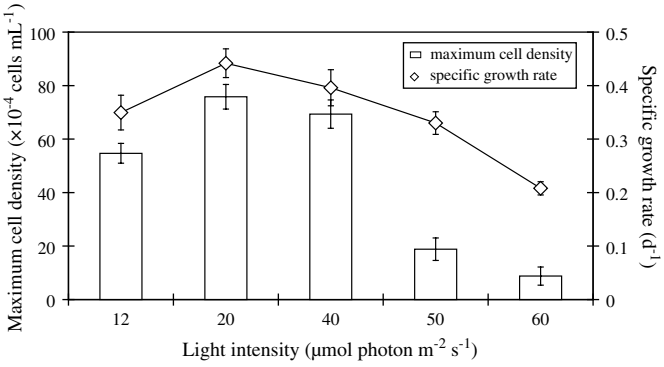

Fig. 6. Effect of light intensity on maximum cell density and specific growth rate of *H. pluvialis*.

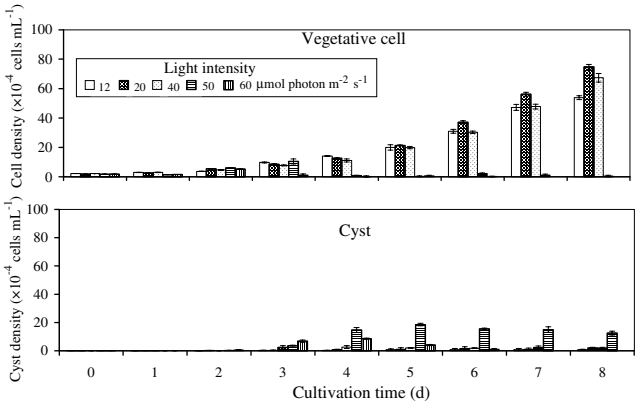

Fig. 7. Density of vegetative cells and cysts of *H. pluvialis* from the operation at different light intensities.

3.8. Semi-continuous culture of H. pluvialis in airlift bioreactor

Semi-continuous cultivation was conducted in order to examine the potential of having a large-scale cultural system that could operate economically. This cultivation was carried out under the most suitable conditions obtained from the aforementioned experiments, i.e. $A_d/A_r = 3.2$, $u_{sg} = 0.4$ cm s^{-1}, light intensity = 20 μmol photon m^{-2} s^{-1} (Fig. 8). In the batch culture, the cell density was allowed to increase until it reached a maximum of 79.5×10^4 cells mL^{-1}, which occurred at about day 6–8 of cultivation. For the semi-continuous culture, the cultivation was started as a batch culture with the initial cell density of 2×10^4 cells mL^{-1}. The cell was grown in the system until it reached the exponential growth phase after which a 50% by volume of culture broth was replaced with a fresh culture medium. The harvest cell density was approximately 40×10^4 cells mL^{-1}. It was proven that with this harvesting cycle, the cell could maintain its vegetative form and in each 4 day cycle, cell density increased up to the level obtained in the previous cycle. The specific growth rate and productivity of semi-continuous culture were 0.31 d^{-1} and 5.52 cells mL^{-1} d^{-1}, respectively. This result

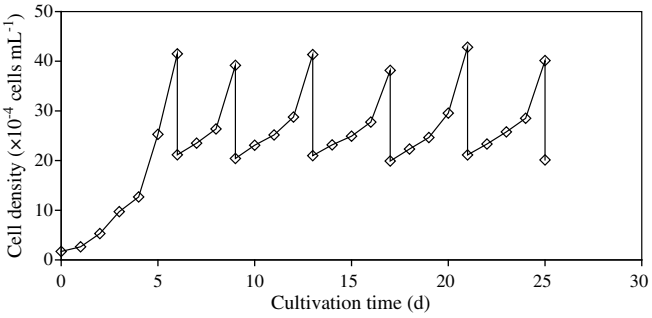

Fig. 8. Cultivation of *H. pluvialis* under semi-continuous culture.

was comparable to that reported by Hata et al. (2001) who successfully achieved the semi-continuous culture, but only in the small scale (in 500 mL Erlenmeyer flask) with a productivity of 6.8 cells mL^{-1} d^{-1}.

4. Conclusions

This work demonstrated that an airlift system was suitable for the cultivation of *H. pluvialis*, one of the most effective microorganisms that could produce high potential antioxidant carotenoid, astaxanthin. The finding well complemented most of the previous reports, which focused mainly on the induction of astaxanthin from this specific strain. Not only was the success in batch culture illustrated, but the airlift system was also proven to deliver a very high productivity of such alga even with the semi-continuous mode of operation. Although the system employed in this work was rather small, the results positively suggested that the upscale investigation for this particular system was highly attractive.

Acknowledgements

The authors greatly appreciate Thailand Research Funds for supporting this work.

References

Boussiba, S., Vonshak, A., 1991. Astaxanthin accumulation in the green alga *Haematococcus pluvialis*. Plant Cell Physiol. 32 (7), 1077–1082.

Chen, F., Chen, H., Gong, X., 1997. Mixotrophic and heterotrophic growth of *Haematococcus lacustris* and rheological behavior of the cell suspensions. Bioresour. Technol. 62, 19–24.

Choi, S.L., Suh, I.S., Lee, C.G., 2003. Lumostatic operation of bubble column photobioreactors for *Haematococcus pluvialis* cultures using a specific light uptake rate as a control parameter. Enzyme Microb. Technol. 33, 403–409.

Fábregas, J., Dominguez, A., Alvarez, D.G., Lamela, T., Otero, A., 1998. Induction of astaxanthin accumulation by nitrogen and magnesium deficiencies in *Haematococcus pluvialis*. Biotech. Lett. 20 (6), 623–626.

Fischer, U., Alfermann, A.W., 1995. Cultivation of photoautotrophic plant cell suspensions in the bioreactor: influence of culture conditions. J. Biotechnol. 41, 19–28.

Gong, X., Chen, F., 1997. Optimization of culture medium for growth of *Haematococcus pluvialis* (Chlorophyceae). Phycology 30, 829–833.

Gong, X., Chen, F., 1998. Influence of medium components on astaxanthin content and production of *Haematococcus pluvialis*. Process Biochem. 33 (4), 385–391.

Grunewald, K., Hagen, C., Braune, W., 1997. Secondary carotenoid accumulation in flagellates of the green alga *Haematococcus pluvialis*. Phycology 32, 378–392.

Gudin, C., Chaumont, D., 1991. Cell fragility—The key problem of microalgae mass production in closed photobioreactor. Bioresour. Technol. 38, 145–151.

Harker, M., Tsavalos, A.J., Yong, A.J., 1996. Autotrophic growth and carotenoid production of in 30 liter air-lift photobioreactor. J. Ferment. Bioeng. 82 (2), 113–118.

Hata, N., Ogbonna, J.C., Hasegawa, Y., Taroda, H., Tanaka, H., 2001. Production of astaxanthin by *Haematococcus pluvialis* in a sequential heterotrophic–photoautotrophic culture. J. Appl. Phycol 13, 395–402.

Johnson, E.A., An, G.H., 1991. Astaxanthin from microbial source. Crit. Rev. Biotech. 11, 297–326.

Kobayashi, M., Kakizono, T., Nagai, S., 1991. Astaxanthin production by green algal, *Haematococcus pluvialis* accompanied with morphological changes in acetate media. J. Ferment. Bioeng. 71 (5), 335–339.

Kobayashi, M., Kakizono, T., Nishio, N., Nagai, S., 1992. Effects of light intensity, light quality, and illumination cycle on astaxanthin formation in a green alga, *Haematococcus pluvialis*. J. Ferment. Bioeng. 74, 61–63.

Krichnavaruk, S., Pavasant, P., 2002. Analysis of gas–liquid mass transfer in an airlift contactor with perforated plates. Chem. Eng. J. 89, 203–211.

Lorenz, R.T., Cysewski, G.R., 2000. Commercial potential for *Haematococcus* microalgae as a natural source of astaxanthin. TIBTECH. 18, 160–165.

Merchuk, J.C., Ronen, M., Giris, S., Arad, S.M., 1998. Light/dark cycles in the growth of the red microalga *Porphyridium* sp. Biotechnol. Bioengng. 59, 705–713.

Pringsheim, E.G., 1996. Nutritional requirements of *Haematococcus pluvialis* and related species. Phycology 2, 1–7.

Sarada, R., Tripathi, U., Ravishankar, G.A., 2002. Influence of stress on astaxanthin production in *Haematococcus pluvialis* grown under different culture conditions. Process Biochem. 37, 623–627.

Tjahjono, A.E., Kakizono, T., Hayama, Y., Nishio, N., Nagai, S., 1994. Isolation of resistant mutants against carotenoid biosynthesis inhibitors for a green alga *Haematococcus pluvialis*, and their hybrid formation by protoplast fusion for breeding of higher astaxanthin producers. J. Ferment. Bioeng. 77 (4), 352–357.

Tripathi, U., Rao, S.R., Ravishankar, G.A., 2002. Biotransformation of phenylprpanoid compoundsto vanilla flavor metabolites in culture of *Haematococcus pluvialis*. Process Biochem. 38, 419–426.

Tung, H.L., Tu, C.C., Chang, Y.Y., Wu, W.T., 1998. Bubble characteristics and mass transfer in an airlift reactor with multiple net draft tubes. Bioprocess. Eng. 18, 323–328.

Zhang, X.W., Gong, X.F., Chen, F., 1999. Dynamics and stability analysis of the growth and astaxanthin production system of *Haematococcus pluvialis*. Ind. Microb. Biotechnol. 23, 133–137.

ภาคผนวก 4

"Enhanced productivity of *Chaetoceros calcitrans* in airlift photobioreactors" Sontaya Krichnavaruk, Sorawit Powtongsook, Prasert Pavasant, Bioresource Technology 98 (2007), 2123-2130

Available online at www.sciencedirect.com
ScienceDirect
Bioresource Technology 98 (2007) 2123–2130
BIORESOURCE TECHNOLOGY

Enhanced productivity of *Chaetoceros calcitrans* in airlift photobioreactors

Sontaya Krichnavaruk [a], Sorawit Powtongsook [b], Prasert Pavasant [a,*]

[a] *Department of Chemical Engineering, Faculty of Engineering, Chulalongkorn University, Bangkok 10330, Thailand*
[b] *Marine Biotechnology Research Unit (at Chulalongkorn University), National Center of Genetic Engineering and Biotechnology, Bangkok 10330, Thailand*

Received 1 May 2006; received in revised form 22 August 2006; accepted 23 August 2006
Available online 10 October 2006

Abstract

The various modes of cultivation of *Chaetoceros calcitrans* in airlift photobioreactors (ALPBRs) were examined. The batch system illustrated that the airlift configuration was superior to the bubble column as the airlift supported the circulation of the cell within the system, leading to a better light utilization. The cultivations in both semi-continuous and continuous systems resulted in a high cell productivity, although the steady state cell concentrations in both systems were lower than that obtained from the batch system. The behavior of the large-scale airlift system was not significantly different from the conventional bubble column where the diatom could only be produced at low cell density. Despite this, among all of the systems investigated in this work, the large-scale system gave the highest productivity. The main limiting factor for the large-scale airlift culture was the availability of light. Based on economical analysis, the continuous cultivation in the 2.8 L ALPBR with a medium feed rate of 3 mL min^{-1} was most attractive where the operation cost could be maintained at a minimum of approx. 7.95×10^{-4} THB L^{-1} h^{-1}. However, this continuous small-scale system still suffered from relatively low cell productivity (8.10×10^4 cells s^{-1}).

Keywords: Airlift photobioreactor; *Chaetoceros calcitrans*; Semi-continuous system; Continuous system; Large-scale system

1. Introduction

The diatom *Chaetoceros calcitrans* has been widely used as a feed in marine hatcheries, especially in feeding shrimp larvae. The diatom is about 4–10 μm in diameter with the box like shape and posses two long pairs of setae. The diatom is an important source of natural polyunsaturated fatty acids (PUFAs) necessary for the growth and immune function of the larvae (Belay, 1997; Borowitzka, 1999; Chiou et al., 2001). Conventionally, the cultivation of *C. calcitrans* started with the controlled cultivation in a small-scale 1 L glass bottle where a high cell density culture of approx. 2×10^6 cells mL^{-1} could be obtained. The culture was scaled up as a low density culture at a concentration of about 2×10^5 cells mL^{-1} in larger tanks or opened ponds with a size of 2–10 m^3 until it was ready to use as feed for marine hatcheries. However, this system experienced difficulties due primarily to contamination as its low specific growth rate might provide enough time for the growth of the unneeded species which may eventually inhibit the growth of the diatom and cause harmful effects to marine culture. Although very few investigations focused on the development of photobioreactors for *C. calcitrans*, several types of closed photobioreactors have so far been introduced for the cultivation of microalgae such as tubular photobioreactor (del Campo et al., 2001; Grima et al., 1996; Lee and Low, 1991; Richmond et al., 1993; Tredici and Zittelli, 1998), vertical alveolar panel (Tredici et al., 1991) and flat plate bioreactor (Göksan et al., 2001; Richmond and Cheng-Wu, 2001; Richmond and Zou, 1999). Recently, we proposed the use of airlift photobioreactor (ALPBR) as an alternative cultivation system

* Corresponding author. Tel.: +66 2 2186870; fax: +66 2 2186877.
E-mail address: prasert.p@chula.ac.th (P. Pavasant).

0960-8524/$ - see front matter © 2006 Elsevier Ltd. All rights reserved.
doi:10.1016/j.biortech.2006.08.010

for *C. calcitrans* where a high maximum cell concentration of 8.88×10^6 cells mL^{-1} could be achieved from the batch cultivation (maximum specific growth rate $= 7.41 \times 10^{-2}$ h^{-1} at $u_{sg} = 3$ cm s^{-1}) (Krichnavaruk et al., 2005). Similar airlift system was also proposed for the high-density cultivation of *Haematococcus pluvialis* where a high specific growth rate of 0.31 d^{-1} was observed (Kaewpintong et al., 2007). Nevertheless, all of these work only focused on batch cultivation which is often encountered drawbacks regarding the production scheduling, reactor maintenance, etc. The aim of this work was therefore to investigate the effect of modes of operation for the cultivation of *C. calcitrans* in various types of ALPBR, i.e. batch, semi-continuous, continuous and the large-scale cultivations.

2. Methods

2.1. Preparation of culturing strain

The inoculum was prepared aseptically. Firstly, the diatom was screened as a single cell and inoculated in the 3 mL test tubes in the standard F/2 medium (Guillard, 1975) for one week. The composition of the medium was (mg L^{-1}) 168.3 $NaNO_3$, 12 $Na_2HPO_4 \cdot H_2O$, 5.8 $FeCl_3 \cdot 6H_2O$, 20 $Na_2EDTA \cdot 2H_2O$, 66 $Na_2SiO_3 \cdot 9H_2O$, 1.96 $CuSO_4 \cdot 5H_2O$, 4.40 $ZnSO_4 \cdot 7H_2O$, 1.26 $Na_2MoO_4 \cdot 2H_2O$, 36 $MnCl_2 \cdot 4H_2O$, 2.0 $CoCl_2 \cdot 6H_2O$, 0.4 vitamin B_1, and (μg L^{-1}) 2 vitamin B_{12}, 100 biotin. Next, the culture was scaled up from 250 to 500 mL flasks where dense cell culture was obtained and used as an inoculum in the airlift photobioreactor (ALPBR).

2.2. Cultivation in ALPBRs

ALPBRs employed in this investigation were of concentric type (Fig. 1a) with dimensions as shown in Table 1. The column was made of clear acrylic plastic to allow effective light penetration and a clear visual observation. The cylindrical draft tube was located concentrically to the outer column with 5 cm space provided at the bottom for liquid circulation. Compressed air was supplied through a porous sparger located centrally at the base of the column and gas flow rate was measured using a calibrated rotameter. Note that the gas flow rate was converted to superficial gas velocity (u_{sg}) based on the area of riser. Fluorescent light bulbs were supplied on both sides of the column as a light source for photosynthesis.

2.3. Determination of cell concentration

The cell concentration was determined by using a normal blood cell counting slide, Haemacytometer. The depth of the counting grid and the area were 0.1 mm and 25 mm^2, respectively. The cells were counted in five large squares on

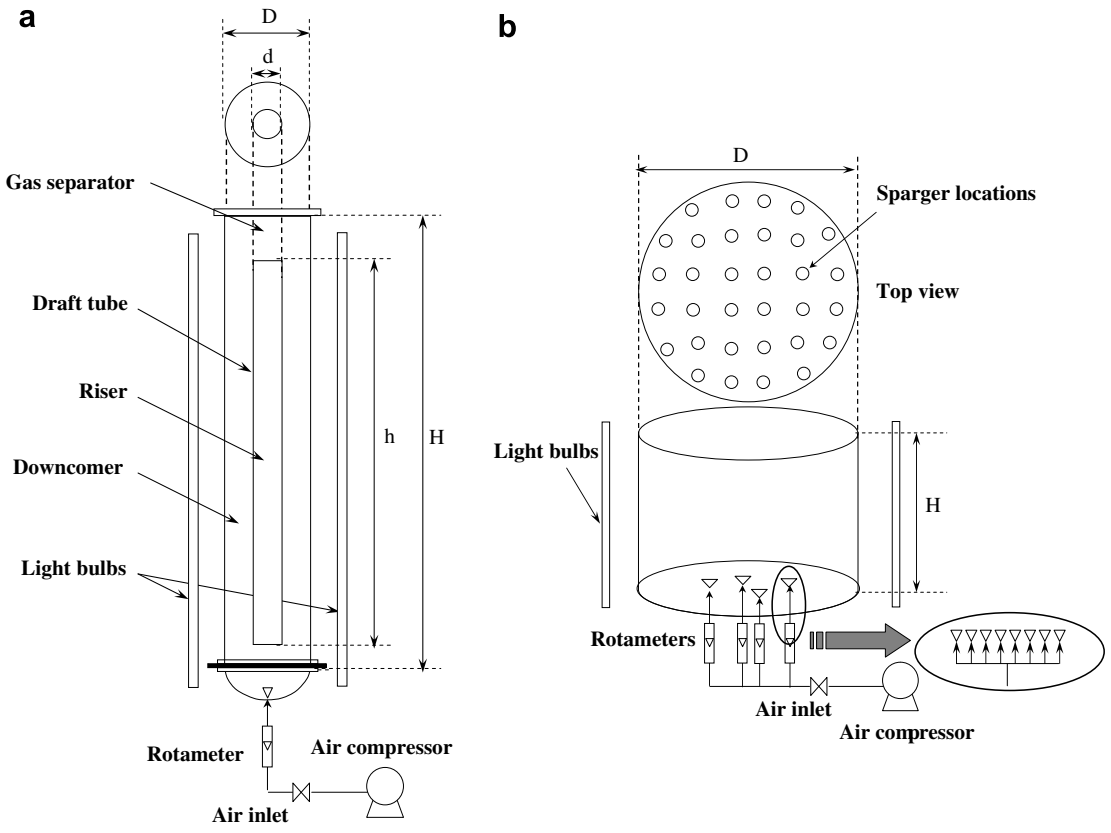

Fig. 1. Experimental setup for the cultivation of *C. calcitrans* (a) 17 L bubble column (BC-1) and 17 L concentric ALPBR (ALPBR-1 and ALPBR-2), (b) 170 L bubble column (BC-2), 170 L concentric ALPBR (ALPBR-3) and 170 ALPBR with multiple draft tube (ALPBR-4).

Table 1
Dimensions of bubble columns and airlift bioreactors employed in this investigation

Type	Working volume (L)	A_d:A_r	Reactor		Draft tube		Number of light source		Light intensity (μmol photon m^{-2} s^{-1})
			Diameter, D (cm)	Height, H (cm)	Diameter, d (cm)	Height, h (cm)	Wall	Top	
BC-1	17	–	15	120	–	–	10 (36 W)	–	384.33
BC-2	170	–	79	66	–	–	16 (18 W)	5 (18 W)	72
ALPBR-1	17	2.62	15	120	8	100	10 (36 W)	–	384.33
ALPBR-2	2.8	1.53	8	66	5	55	5 (36 W)[a]	–	118
ALPBR-3	170	1.47	79	66	50	50	16 (18 W)	5 (18 W)	72
ALPBR-4	170	2.82	79	66	18[b]	40[b]	16 (18 W)	5 (18 W)	72

[a] The light source was supplied perpendicular to the column.
[b] Four draft tubes were placed in the reactor and air was supplied through the porous spargers located at the bottom of each draft tube.

the grid (25 small squares per 1 large square) where the cell number was calculated from:

$$N = 5 \times d \times n \times 10^4 \quad (1)$$

where N = cells concentration (cells mL^{-1}), n = number of cells on five large squares (cells), d = dilution factor (–).

2.4. Batch cultivation

The batch cultivation of *C. calcitrans* was carried out both in the 17 L bubble column (BC-1) and the 17 L airlift photobioreactor (ALPBR-1). Fresh sea water (30 ppt) was added into the systems along with the F/2 medium. The inoculum was then added with the initial cell concentration of approx. 1×10^5 cells mL^{-1}. Compressed air was supplied through a porous sparger with $u_{sg} = 3$ cm s^{-1}, which was the optimal gas flow rate (Krichnavaruk et al., 2005). Five 36 W fluorescent light bulbs were supplied on both sides of the column as the light source for photosynthesis with the light intensity at the outer column of approx. 350 μmol photon m^{-2} s^{-1}. Temperature was controlled at around 30 (±2 °C). Samples were collected at every 3 h for the measurement of cell concentration. The specific growth rate was calculated from the following equation:

$$\mu = \frac{\ln(N_2) - \ln(N_1)}{t_2 - t_1} \quad (2)$$

where μ = specific growth rate (h^{-1}), N_1 = cells concentration at t_1 (cells mL^{-1}), N_2 = cells concentration at t_2 (cells mL^{-1}).

2.5. Semi-continuous cultivation

The semi-continuous system was investigated to improve the productivity of the system by using ALPBR-1. Gas velocity was supplied at $u_{sg} = 3$ cm s^{-1} which was the optimal gas velocity as operated in the batch cultivation. The system was initially operated as a batch system and the diatom was left growing for about 30 h until it reached the middle of the exponential growth period where approx. 50% of the culture was harvested. The remaining culture was diluted to approx. 1.2×10^6 cells mL^{-1} by adding fresh sea water. The nutrient stock solutions were then added to the system with the final nutrient concentration adjusted to the standard F/2 medium. The culture was then harvested at every 12 h. The productivity of the diatom for the batch and semi-continuous cultivation was calculated from the following equation:

$$P = \left(\frac{N_2 - N_1}{t_2 - t_1}\right) \times \frac{V \times 1000}{3600} \quad (3)$$

where P = productivity (cells s^{-1}), N_1 = cells concentration at t_1 (cells mL^{-1}), N_2 = cells concentration at t_2 (cells mL^{-1}), V = harvested volume (L).

2.6. Continuous cultivation

The continuous cultivation of *C. calcitrans* was carried out in a smaller scale airlift photobioreactor (ALPBR-2). During the first 30 h of the cultivation, the diatom was operated as a batch system. After this point, fresh sea water mixed with the standard F/2 medium was fed into the system at various volumetric feed rates (2–4 mL s^{-1}). Samples were taken at every 3 h to determine the cell concentration and specific growth rate. The volume of the system was controlled by the overflow outlet at the top of the column. The productivity of the diatom was simply calculated from the following equation:

$$P = QC \tag{4}$$

where P = productivity (cells s^{-1}), Q = volumetric flow rate of fresh medium (mL s^{-1}), C = effluent cell concentration (cells mL^{-1}).

The specific productivity can be calculated as follows:

$$\mathrm{SP} = \frac{P}{V} \tag{5}$$

where SP = specific productivity (cells L^{-1} s^{-1}), P = productivity (cells s^{-1}), V = harvested volume (L).

2.7. Large-scale cultivation

The cultivation of the diatom *C. calcitrans* in the large-scale system was carried out in the conventional bubble column (BC-2), a conventional concentric airlift photobioreactor (ALPBR-3) where a single draft tube with 50 cm diameter (d) and 50 cm height (h) was inserted concentrically into the outer column, and a multiple draft tubes airlift photobioreactor (ALPBR-4) with four draft tubes, each with a diameter (d) of 18 cm and a height (h) of 40 cm. Porous spargers were well distributed through the riser area of each system. Both ALPBR-3 and ALPBR-4 were of the same size as that of BC-2, all with a working volume of approx. 170 L. Details of these systems are given Table 1 where a schematic diagram of the main column is provided in Fig. 1b. The initial cell concentration was approx. 0.5×10^6 cells mL^{-1}. Due to the limitation of the air compressor for this large-scale column, gas flow rate was controlled and fixed at 250 mL s^{-1}. Sixteen fluorescent light bulbs (18 W each) were supplied around the tank, and also five bulbs on the top section for photosynthesis. Light intensity around the wall and at the surface was around 48–52 μmol photon m^{-2} s^{-1}. Samples were collected at every 3 h for the measurement of cell concentration and the calculation of specific growth rate.

3. Results and discussion

3.1. Batch culture

The growth behavior of *C. calcitrans* in the airlift system clearly outperformed that in the bubble column (BC-1) as the cultivation in the airlift system (ALPBR-1) provided almost a twofold productivity of the diatom than that in the bubble column (8.88×10^6 cells mL^{-1} in the airlift when compared with 4.96×10^6 cells mL^{-1} in the bubble column). This was also apparent in the specific growth rate which was around 0.074 h^{-1} in the airlift system, whereas only about 0.029 h^{-1} was reached in the bubble column. The reason for this could be due to the differences in liquid flow behavior in both systems. In ALPBR, the diatom was carried along the column height due to the energy transfer from gas bubbles. As the bubbles were separated from the liquid at the top surface, the heavier liquid and the diatom moved down the column in the downcomer section and re-entered the riser through the space provided at the bottom of the system. This circulation allowed the diatom to constantly move to the "high light intensity" area, i.e. in downcomer section. Apparently, this was beneficial for photosynthesis of the diatom. In the case of bubble column, the movement of liquid was random as the liquid and bubbles were completely mixed in one chamber. The low liquid velocity condition did not support a proper circulation of the diatom, and the sedimentation of the diatom could, at times, be observed at the bottom of the column. Therefore the diatom could not be exposed to high light intensity, and hence, ineffective photosynthesis was resulted and this led to a low productivity.

The growth of the diatom in the airlift system with an initial cell concentration of approx. 1×10^5 cells mL^{-1} ($u_{sg} = 3$ cm s^{-1}) started with a 9 h lag phase, after which the diatom entered its exponential growth period where the cell concentration rapidly increased before reaching the stationary phase where the maximum cell density was approx. 8.88×10^6 cells mL^{-1}. This growth process reached the maximum cell concentration in 44 h which rendered a specific growth rate of about 7.41×10^{-2} h^{-1}. This was equivalent to a productivity of 9.42×10^5 cells s^{-1} or a specific productivity of 5.54×10^4 cells L^{-1} s^{-1}.

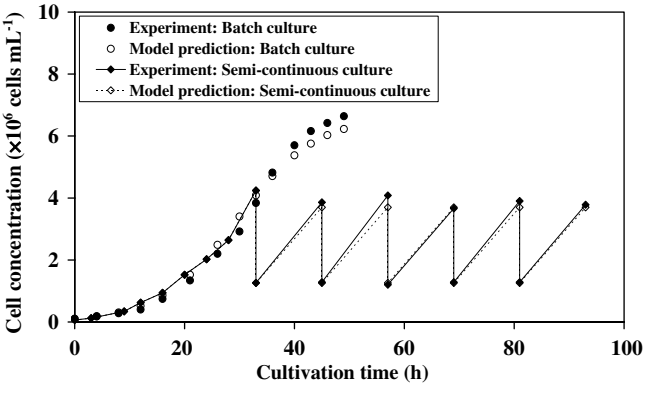

Fig. 2. Comparison between growth behavior of *C. calcitrans* for the cultivation in batch and semi-continuous culturing system (ALPBR-1 with $u_{sg} = 3$ cm s^{-1}) and growth behavior from model prediction.

3.2. Semi-continuous culture

The batch cultivation, although provided a relatively high final cell concentration, often suffered from an initially slow growth regime, not to mention the loss of time during the final system cleansing. The cultivation of *C. calcitrans* in the semi-continuous system was, therefore, investigated to examine the probability of enhancing the productivity of the diatom. Fig. 2 illustrates the result for the cultivation of *C. calcitrans* in the 17 L semi-continuous system. An average maximum cell concentration achieved from each cycle (12 h) was around 3.86×10^6 cells mL^{-1} with a specific growth rate of about 9.25×10^{-2} h^{-1}. The cultivation of the diatom in the semi-continuous system achieved an average productivity of approx. 7.19×10^5 cells s^{-1} or equivalent to a specific productivity of 5.99×10^4 cells L^{-1} s^{-1} which was marginally higher than those obtained from the batch system. Summary of the performance of the different systems employed in this work is provided in Table 2.

3.3. Prediction of airlift system performance

The prediction of system performance for batch and semi-continuous cultures in ALPBR-1 could be achieved through the following derivations. For the batch system, the mass balance around the reactor results in:

$$V\frac{dx(t)}{dt} = \mu x(t)V \tag{6}$$

The Logistic law (Bailey and Ollis, 1986) was assumed to explain the growth rate of the diatom where

$$\mu = \mu_m\left(1 - \frac{x(t)}{x_m}\right) \tag{7}$$

Substituting Eq. (7) into Eq. (6) yields:

$$V\frac{dx(t)}{dt} = \mu_m\left(1 - \frac{x(t)}{x_m}\right)x(t)V \tag{8}$$

This could be integrated to:

$$x(t) = \frac{x_0 x_m e^{\mu_m t}}{x_m - x_0 + x_0 e^{\mu_m t}} \tag{9}$$

where $x(t)$ = cell concentration (cells mL^{-1}), x_0 = cell concentration (cells mL^{-1}), x_m = maximum cell concentration (cells mL^{-1}), t = culturing time (h), μ = specific growth rate (h^{-1}), μ_m = maximum specific growth rate (h^{-1}), V = cultivating volume (L).

The maximum cell concentration (x_m) and the maximum specific growth rate (μ_m) were system dependent and were, therefore, obtained from the experiment in the batch cultivation, and in this case, these two parameters were 6.64×10^6 cells mL^{-1} and 1.4×10^{-1} h^{-1}, respectively. Eq. (9) was then used to simulate the growth curve of the diatom in both batch and semi-continuous modes. Fig. 2 illustrates that the model predictions agreed reasonably well with experimental results. For the simulation of the semi-continuous culture, the initial cell concentration for each cycle was controlled at approx. 1.2×10^6 cells mL^{-1} and the harvesting period was maintained at 12 h. The model was then used to estimate the cell concentration in each harvesting cycle. The predicted productivity of the semi-continuous system using this model was 6.32×10^5 cells s^{-1}, which was slightly lower than the actual level of 7.19×10^5 cells s^{-1}. This was equivalent to an error of approx. 12%.

The model was further implemented to predict the harvesting period for which the maximum productivity could be achieved in both batch and semi-continuous systems. The maximum productivity for the batch operation was predicted by using the following correlations:

$$\text{Productivity} = \left(\frac{x(t) - x_0}{t - t_0}\right) \times V \tag{10}$$

To obtain the maximum productivity, the time differentiation of Eq. (10) must be equal to zero:

$$V\frac{d}{dt}\left(\frac{x(t) - x_0}{t}\right) = 0 \tag{11}$$

Substitution of Eq. (9) into Eq. (11) yielded:

$$V\frac{d}{dt}\left(\frac{\dfrac{x_0 x_m e^{\mu_m t}}{x_m - x_0 + x_0 e^{\mu_m t}} - x_0}{t}\right) = 0 \tag{12}$$

Table 2
Comparison between maximum cell concentration, productivity, specific productivity and specific growth rate for the cultivation of *Chaetoceros calcitrans* in BCs and ALPBRs in various modes of operation

Systems	Harvest time (h)	Maximum cell concentration (cells mL^{-1})	Productivity (cells s^{-1})	Specific productivity (cells L^{-1} s^{-1})	Specific growth rate (h^{-1})
Batch BC-1	60	4.96×10^6	3.83×10^5	2.25×10^4	2.88×10^{-2}
Batch ALPBR-1	44	8.88×10^6	9.42×10^5	5.54×10^4	7.41×10^{-2}
Semi-continuous ALPBR-1	>12	3.86×10^6	7.19×10^5	5.99×10^4	9.25×10^{-2}
Continuous[a] ALPBR-2	>30	1.62×10^6	8.10×10^4	2.89×10^4	6.42×10^{-2}
Large-scale BC-2	80	2.51×10^6	1.21×10^6	7.12×10^3	2.46×10^{-2}
Large-scale ALPBR-3	80	2.96×10^6	1.48×10^6	8.68×10^3	2.58×10^{-2}

[a] Continuous culturing system with a medium feed rate of 3 mL min^{-1}.

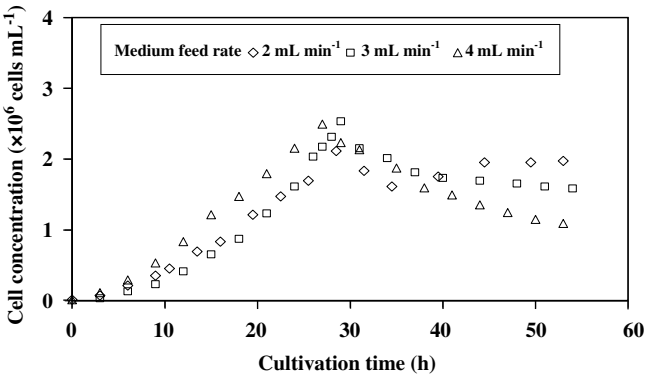

Fig. 3. Growth behaviors of *C. calcitrans* in continuous culturing system with various medium feed rates (ALPBR-2 with $u_{sg} = 3$ cm s^{-1}).

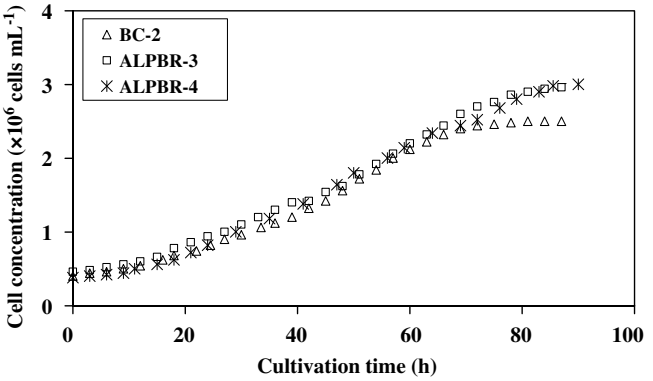

Fig. 4. Growth curves of *C. calcitrans* in large-scale systems (BC-2, ALPBR-3 and ALPBR-4 with $u_{sg} = 1$ cm s^{-1}).

Eq. (12) suggested that the maximum productivity of 6.35×10^5 cells s^{-1} would be obtained if the system was allowed to operate for 41 h, and with $x_0 = 1.03 \times 10^5$ cells mL^{-1}.

For the semi-continuous cultivation, the maximum productivity can be calculated from:

$$\frac{d}{dt}\left(\frac{x(t) - x_0}{t - t_0}\right)(V_0 - V(t)) = 0 \quad (13)$$

where V_0 = initial cultivating volume (L), $V(t)$ = remaining volume after the harvest (L).

From the balance of component x;

$$V_0 x_0 = V(t)x(t) \quad (14)$$

$$V(t) = \frac{V_0 x_0}{x(t)} \quad (15)$$

Eqs. (9) and (15) were substituted into Eq. (13), which allowed the determination of the cycle time required to yield the maximum productivity (with $V_0 = 17$ L and $x_0 = 1.26 \times 10^6$ cells mL^{-1}). In this case, it was predicted that the maximum productivity of 7.22×10^5 cells s^{-1} could be achieved after 19 h of cultivating period. However, this predicted maximum productivity was quite close to the actual attainable productivity with 12 h cultivation.

3.4. Continuous culture

This section focused on the continuous cultivation of the diatom *C. calcitrans* in ALPBR-2. As the system was switched to the continuous mode, the cell concentration started to drop due to the dilution effect (see Fig. 3). After another 10 h or so, the steady state could be observed. The cultivation of the diatom with the nutrient feed rates of 2, 3 and 4 mL min^{-1} resulted in the dilution rates of 4.29×10^{-2}, 6.43×10^{-2} and 8.57×10^{-2} h^{-1}, respectively. The maximum final cell concentration of approx. 1.95×10^6 cells mL^{-1} was obtained at the feed rate of 2 mL min^{-1}. At this condition, the attainable specific productivity was 2.32×10^4 cells L^{-1} s^{-1} (or equivalent to a productivity of 6.5×10^4 cells s^{-1}). Due to a higher dilution effect, the maximum steady state cell concentration for the cultivation at the medium feed rate of 3 mL s^{-1} was only 1.62×10^6 cells mL^{-1}. Although this value was lower than that obtained from the case with the medium feed rate of 2 mL^{-1}, the productivity was higher at approx. 8.10×10^4 cells s^{-1} or equivalent to a specific productivity of 2.89×10^4 cells L^{-1} s^{-1}. For the case where the medium feed rate was maintained at 4 mL min^{-1}, the final cell concentration was unable to reach the steady state concentration as the diatom seemed to be continually diluted by the feed of nutrient. In conclusion, for the range of operating condition employed in this work, the continuous ALPBR system should be conducted with the nutrient feed rate of 3 mL min^{-1} to ensure the highest level of cell productivity.

3.5. Large-scale cultivation

Conventionally, the diatom *C. calcitrans* was cultivated in a large-scale pond. The main reason for this was perhaps the economic of scale as a large-scale system often requires a lower investment when compared to small systems with the same volume. This section examined the performance of such system compared with that of smaller systems. This was to investigate whether the large-scale cultivation was, in fact, suitable to the growth of the diatom.

The results from the cultivation of *C. calcitrans* in the large-scale system was illustrated in Fig. 4. It was found that the maximum cell concentration of the diatom in ALPBR-3 (2.96×10^6 cells mL^{-1}) and in ALPBR-4 (3.04×10^6 cells mL^{-1}) were slightly higher than that from BC-2 (2.51×10^6 cells mL^{-1}). However, the specific growth rate of the diatom in the large-scale cultivation for the cultivation in bubble column and in both ALPBRs was not significantly different, i.e. $\mu = 2.46 \times 10^{-2}$ h^{-1} for BC-2, 2.58×10^{-2} h^{-1} for ALPBR-3 and 2.52×10^{-2} h^{-1} for ALPBR-4. It was reported that there existed non-ideal flow particularly in airlift systems with large riser where the internal circulation took place within the riser itself (Wongsuchoto et al., 2003). This local circulation caused the system to behave like a bubble column. Therefore, in ALPBR-4, the riser was divided into four sub-sections, each with a smaller diameter. This was to minimize the local circulation in the riser and a better liquid circulation within the system was anticipated.

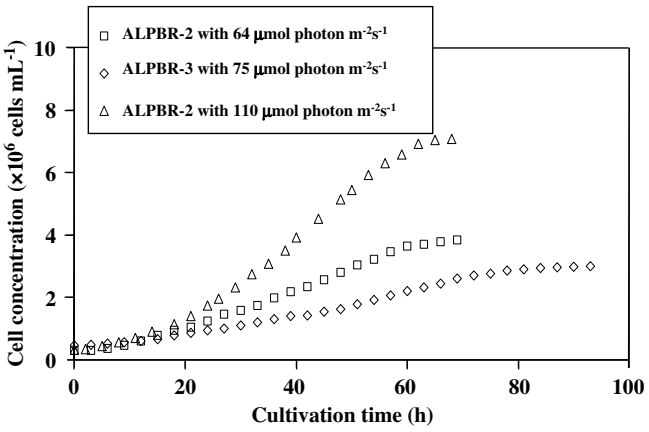

Fig. 5. Comparison between the growth of *C. calcitrans* in ALPBR-2 (initial cell concentration of approx. 3×10^5 cells mL^{-1}, $u_{sg} = 3$ cm s^{-1}) with the variation in light intensity and the cultivation in ALPBR-3.

However, the large system was limited by the capacity of the air pump and the maximum aeration rate of 250 mL s^{-1} could only be achieved. Therefore, under the operating conditions employed in this work, the difference in the behaviors of the three systems might not be enough to have significant effect on the growth of the diatom, as obvious from the resulted mentioned above. The cultivation of the diatom in these large-scale systems was demonstrated to increase the productivity of the diatom. This was mainly due to the increase in the harvested volume when compared to the small systems.

3.6. Limiting factors for the operation in large-scale systems

One of the main drawbacks for the cultivation of the diatom in large-scale systems was the poor light utilization. The light source could only be supplied around the wall and at the top of the tank, and with this setup, the light intensities measured in the system were around 48–50 μmol photon m^{-2} s^{-1} near the inner wall, 72 μmol photon m^{-2} s^{-1} at the outer wall, 52 μmol photon m^{-2} s^{-1} near the surface of liquid level, and approx. 30 μmol photon m^{-2} s^{-1} at the center of the tank. In particular, when the cells grew high in density, poor light penetration became a serious problem that retarded the effective growth of the diatom.

To further investigate the effect of light intensity on the growth of the diatom, the cultivation of the diatom was carried out in a smaller scale 2.8 L ALPBR (ALPBR-2) at similar light intensity levels to the large tank. Fig. 5 demonstrates the comparison between the cultivation in these two different scale ALPBRs. It was obvious that the growth rate in ALPBR-3 at the light intensity (at the wall) of 75 μmol photon m^{-2} s^{-1} was even lower than that in ALPBR-2 with the light intensity of 64 μmol photon m^{-2} s^{-1}. However, it should be mentioned that the ability of the passage of light through the large-scale system was much lower than that in the small-scale system. Therefore the higher light intensity at the wall in the large-scale system did not necessarily mean that the light intensity would remain high within the culture. Unlike the large system, the light intensity in the small-scale system should remain almost constant throughout the column. Nevertheless, as the performance of ALPBR-2 with low light intensity became closer to that of ALPBR-3 at the same range of light intensity, this suggested that the findings in the small-scale could, to some extent, be used to explain the phenomena within the large-scale system.

Fig. 5 also revealed that the light intensity could significantly affect the growth of the diatom, and in this case, the greater final cell density of around 7.08×10^6 cells mL^{-1}

Table 3
Economical analysis for the cultivation of 1×10^{12} cells of *Chaetoceros calcitrans* in ALPBRs

		Working volume			
		Batch (ALPBR-1)	Semi-continuous (ALPBR-1)	Continuous[a] (ALPBR-2)	Large-scale (ALPBR-3)
Effective volume (L)	[*A*]	17	12	–	170
Cycle time (h)	[*B*]	44	12	–	80
Productivity[b] (cells s^{-1})	[*C*]	9.42×10^5	7.19×10^5	8.10×10^4	1.48×10^6
Specific productivity[b] (cells L^{-1} s^{-1})	[*D*]	5.54×10^4	5.99×10^4	2.89×10^4	8.68×10^3
Cultivation time (h)	$[E = (1 \times 10^{12} \times 3600) \div C]$	295	386	3429	188
Number of cycle (–)	$[F = E \div B]$	6.70	32.17	–	2.35
Total volume of sea water used (L)	$[G = A \times F]$	114	386	617	400
Cost of water, 0.06 THB L^{-1} (THB)	$[H = 0.06 \times G]$	6.84	23.16	37.03	23.97
Cost of nutrient, 1 THB L^{-1} (THB)	$[I = G \times 1]$	114	386	617	400
Power of air compressor (W)	[*J*]	300	300	60	1600
Power of light source (W)	[*K*]	400	400	40	378
Total electrical unit (units)	$[L = (J + K) \times E \div 1000]$	207	270	343	372
Electrical cost, 3 THB per unit (THB)	$[M = 3 \times L]$	620	811	1029	1116
Total investment cost (THB)	$[N = H + I + M]$	740	1220	1683	1539
Investment cost per hour (THB h^{-1})	$[O = N \div E]$	2.51	3.16	0.49	8.19
Specific investment cost (THB L^{-1} h^{-1})	$[P = O \div G]$	2.20×10^{-2}	8.19×10^{-3}	7.95×10^{-4}	2.05×10^{-2}

[a] Continuous cultivation with a medium flow rate of 3 mL min^{-1}.
[b] From Table 2.

with $4.24 \times 10^{-2}\ h^{-1}$ specific growth rate was obtained at the light intensity of 110 μmol photon $m^{-2}\ s^{-1}$ whereas the lower light intensity (64 μmol photon $m^{-2}\ s^{-1}$) yielded a much lower cell concentration of 3.84×10^6 cells mL^{-1} ($3.42 \times 10^{-2}\ h^{-1}$ specific growth rate). This finding implied that insufficient light intensity could negatively affect the performance, and this was the case of the large-scale system, and as long as the light intensity could not be maintained at higher level (without causing excessive heat), the cultivation in the large-scale system could only be subject to low cell density.

3.7. Economics of cultivation systems for C. calcitrans

The economical analysis for the cultivation of the diatom *C. calcitrans* in various scales of ALPBRs was carried out where the results are shown in Table 3. The systems involved in this analysis were the batch cultivation (ALPBR-1), semi-continuous cultivation (ALPBR-1), continuous cultivation (ALPBR-2) and the large-scale cultivation (ALPBR-3). This analysis was based on the production of 1×10^{12} cells. It was observed that the most attractive system for the cultivation of the diatom in marine hatcheries was the continuous cultivation of the diatom in the 2.8 L ALPBR (ALPBR-2) with the medium feed rate of 3 mL min^{-1}. The lowest operating cost, approx. 7.95×10^{-4} THB $L^{-1}\ h^{-1}$, was obtained which was the lowest when compared to any other systems. Surprisingly, the productivity of this system was found to be the lowest among the four systems. The benefits of this system were derived from a number of advantages when compared to the larger systems, i.e. low overhead charge due to the labor cost, minimal lost of time during the start up and shut down period or for system maintenance. As the cells remained active at all time in the continuous system, the culture medium could be switched to the new reactor as soon as the maintenance was needed without disturbing the growth of the diatom. The maintenance and equipment costs in this system, i.e. reactor, air compressor and light source, were also lower than the setup for larger systems.

4. Conclusions

This investigation described the achievement in the cultivation of *C. calcitrans* in various reactor modes. It was found that the semi-continuous and the continuous systems could be successfully implemented to minimize the maintenance of the batch system. The large-scale system was also practiced, but could only reach a small final cell concentration. Due to the size of the harvested volume, the large-scale was found to produce cell at the highest productivity. The main drawback for this large system was the limitation on the availability of light, which restricted the growth of the diatom. The economical analysis pointed out that small culture system running in continuous mode seemed to be the most attractive choice for the cultivation of *C. calcitrans*.

Acknowledgements

The author would like to acknowledge the Thailand Research Fund (TRF) for their financial support.

References

Bailey, J.E., Ollis, D.F., 1986. Biochemical Engineering Fundamentals. McGraw-Hill, New York.

Belay, A., 1997. Mass cultivation of *Spirulina* outdoors—the earthrise farms experience. In: Vonshakm, A. (Ed.), *Spirulina platensis* (*Arthrospira*): Physiology, Cell Biology and Biotechnology. Taylor and Francis, London, pp. 131–158.

Borowitzka, M.A., 1999. Commercial production of microalgae: ponds, tanks, tubes and fermenter. J. Biotechnol. 70, 313–321.

Chiou, S.Y., Su, W.W., Su, Y.C., 2001. Optimizing production of polyunsaturated fatty acids in *Machantia polymorpha* cell suspension culture. J. Biotechnol. 85, 247–257.

del Campo, J.A., Rodriguez, H., Moreno, J., Vergas, A., Rivas, J., Guerrero, M.G., 2001. Lutein production by *Muriellopsis* sp. in an outdoor tubular photobioreactor. J. Biotechnol. 85, 289–295.

Göksan, T., Durmaz, Y., Gökpinar, S., 2001. Effects of light path lengths and initial culture density on the cultivation of *Chaetoceros muelleri*. Aquaculture 217, 431–436.

Grima, E.M., Sanchez Perez, A.S., Camacho, F.G., Garcia Sanchez, J.L., Acien Fernandez, F.G., Alonso, D.L., 1996. Productivity analysis of outdoor chemostat culture in tubular air-lift photobioreactors. J. Appl. Phycol. 8 (4–5), 369–380.

Guillard, R.L., 1975. Culture of phytoplankton for feeding marine invertebrates (for general algae culture techniques). In: Smith, W.L., Chanley, M.H. (Eds.), Culture of Marine Invertebrates Animal. Plenum Press, New York, pp. 15–41.

Kaewpintong, K., Shotipruk, A., Powtongsook, S., Pavasant, P., 2007. Photoautotrophic high-density cultivation of vegetative cells of *Haematococcus pluvialis* in airlift bioreactor. Bioresource Technol. 98, 288–295.

Krichnavaruk, S., Loataweesup, W., Powtongsook, S., Pavasant, P., 2005. Optimal growth conditions and the cultivation of *Chaetoceros calcitrans* in airlift photobioreactor. J. Chem. Eng. 105, 91–98.

Lee, Y.K., Low, C.S., 1991. Effect of photobioreactor inclination on the biomass productivity of an outdoor algal culture. Biotechnol. Bioeng. 38, 995–1000.

Richmond, A., Boussiba, S., Vonshak, A., Kopel, R., 1993. A new tubular reactor for mass production of microalgae outdoors. J. Appl. Phycol. 5, 327–332.

Richmond, A., Cheng-Wu, Z., 2001. Optimization of a flat plate glass reactor for mass production of *Nannochloropsis* sp. Outdoors J. Biotechnol. 85, 259–269.

Richmond, A., Zou, N., 1999. Efficient utilization of high photon irradiance for mass production of photoautotrophic micro-organisms. J. Appl. Phycol. 11, 123–127.

Tredici, M.R., Carlozzi, P., Zittelli, C.G., Materassi, R., 1991. A vertical alveolar panel (VAP) for outdoor mass cultivation of microalgae and cyanobacteria. Bioresource Technol. 38, 153–159.

Tredici, M.R., Zittelli, G.C., 1998. Efficiency of sunlight utilization: tubular versus flat photobioreactors. Biotechnol. Bioeng. 57 (2), 187–197.

Wongsuchoto, P., Charinpanitkul, Y., Pavasant, P., 2003. Bubble size distribution and gas–liquid mass transfer in airlift contactors. J. Chem. Eng. 92, 81–90.

ภาคผนวก 5

“Influence of salinity on bubble size distribution and gas-liquid mass transfer in airlift contactors”, Duangkamol Ruen-ngam, Porntip Wongsuchoto, Apiradee Limpanuphap, Tawatchai Charinpanitkul, Prasert Pavasant (In-press)

ELSEVIER

Chemical Engineering Journal xxx (2008) xxx–xxx

Chemical Engineering Journal

www.elsevier.com/locate/cej

Influence of salinity on bubble size distribution and gas–liquid mass transfer in airlift contactors

Duangkamol Ruen-ngam, Porntip Wongsuchoto, Apiradee Limpanuphap, Tawatchai Charinpanitkul, Prasert Pavasant *

Department of Chemical Engineering, Faculty of Engineering, Chulalongkorn University, Bangkok 10330, Thailand

Received 12 June 2007; received in revised form 21 December 2007; accepted 26 December 2007

Abstract

The investigation of the effect of salinity on the performance of airlift contactor was achieved using the 17 l internal loop airlift with height of 1.2 m, and 0.137 m diameter. Various draft tubes with different diameter sizes were provided to vary the ratio between downcomer and riser cross-sectional areas (A_d/A_r) from 0.061 to 1.01. The superficial gas velocity (u_{sg}) was supplied in a range from 0.01 to 0.07 m/s and the salinity was adjusted from 0 to 45 ppt. The Sauter mean diameter of the bubble (d_{Bs}) appeared to be smaller in saline water than in fresh water. Bubble size was regulated by two factors. The first one was the hydrophilic repulsive force which inhibited bubble coalescence whereas the second was the Laplace pressure which controlled the coalescence and breakup of bubbles. The range of pressure difference, ΔP, acting on the bubble that promoted bubble coalescence was between 15 and 20 N/m^2 below which bubble coalescence was inhibited and above which bubble breakage prevailed. In saline water, d_{Bs} decreased with u_{sg}. This was caused by the collision and breakup of bubbles at high gas holdup which occurred at ΔP greater than 20 N/m^2. Axial variation in d_{Bs} was only observed at low u_{sg} (less than 0.04 m/s) where bubbles in the bottom section of the airlift were larger than those in the middle and top sections. It was anticipated that the middle and top sections exhibited higher turbulent conditions than the bottom section at this low aeration rate. The effect of draft tube size was quite important where the smallest draft tube (smallest downcomer area) best promoted the breakup of the bubbles with a relatively high ΔP of approximately 50–97 N/m^2. The effect of salinity on the overall volumetric mass transfer coefficient (k_La) was only apparent at high aeration rate where the fresh water provided a higher k_La than the saline water. In fact, the specific area (a) was high in the saline water systems, however, the mass transfer coefficient (k_L) was higher in the fresh water system than saline water. Finally, a general correlation for the estimation of k_L in the airlift system was proposed.

Keywords: Pressure difference; Bubble behavior; Mass transfer; Hydrodynamics

1. Introduction

An airlift system is an example of gas–liquid contacting device for which its application in biotechnology area has grown significantly in recent years [1–4]. Examples include the cultivation of fresh water single cell algae *Haematococcus pluvialis* as proposed by Kaewpintong et al. [5] and the high productivity of the sea water diatom *Chaetoceros calcitrans* in airlift photobioreactors as proposed by Krichnavaruk et al. [6,7]. One of the most significant parameters in the design of such airlift systems is the overall volumetric mass transfer coefficient which is commonly employed to demonstrate the efficiency of oxygen transfer from gas to liquid. This quantity depends on the system geometry and liquid properties which are related to several other parameters. Principally, this parameter is constituted of the mass transfer coefficient (k_L) and the specific interfacial area (a_L) which then depends on the flow regimes, hydrodynamics and bubble characteristics in the system. Information regarding bubble size distribution is often useful as it determines the level of interfacial mass transfer and other hydrodynamic behavior of the systems. However, the availability of such information is quite sparse. Literature reported that bubble breakage was a predominant factor in the gas–liquid contacting devices particularly at high gas throughputs [8–11]. Hence, the systems at high aeration rate are typically operated with smaller bubble size range which enhances gas holdup and consequently gas–liquid mass transfer. Bubble breakage was also found to take place along the height of the column due to an increasing interaction between

* Corresponding author. Tel.: +66 2 218 6870; fax: +66 2 218 6877.
E-mail address: prasert.p@chula.ac.th (P. Pavasant).

1385-8947/$ – see front matter © 2008 Published by Elsevier B.V.
doi:10.1016/j.cej.2007.12.024

Nomenclature

Nomenclature

a	specific interfacial area based on liquid volume (m^2/m^3)
A	cross-sectional area (m^2)
c	dissolved oxygen concentration (mg/l)
c^*	saturated dissolved oxygen concentration concentration (mg/l)
c_L	oxygen concentration in liquid phase (mg/l)
c_o	initial dissolved oxygen concentration (mg/l)
$d_{B,i}$	sphere bubble diameter with the same volume as ellipsoidal bubble (mm)
d_{Bs}	Sauter mean diameter (mm)
D_l	diffusivity (m^2/s)
D_i	inside diameter of draft tube (cm)
D_{io}	outer diameter of draft tube (cm)
h_i	video level (cm)
h	height of defined liquid level in the column (cm)
H_L	unaerated liquid height (m)
H_D	aerated liquid heights (m)
g	gravitational acceleration (m/s^2)
k_g	overall mass transfer coefficient (m/s)
k_L	overall mass transfer coefficient (m/s)
k_La	overall volumetric mass transfer coefficient (l/s)
n_i	occurrence frequency number
p	major axes of bubble images
ΔP	pressure difference acting on bubbles (N/m^2)
ΔP_m	pressure difference between the two measuring ports (N/m^2)
q	minor axes of bubble images
t	time (s)
u_{sg}	superficial gas velocity (m/s)
u_α	terminal rise velocity of bubble (m/s)

Greek symbols

δ	film thickness (cm)
ε_d	downcomer gas holdup
ε_o	overall gas holdup
ε_r	riser gas holdup
μ	viscosity (kg/m s)
ρ	density (kg/m^3)
σ	surface tension (N/m)

bubbles as they traveled up the top of the column [2]. Wongsuchoto et al. [4] reported that bubble breakage occurred more at the top part resulting in smaller bubble size to be smaller than that at the lower part. Electrolyte solutions such as sea water were reported to provide a higher k_La than that in fresh water as the bubble size in such systems was relatively small. On the other hand, systems with higher viscosity such as CMC (carboxymethyl cellulose) exhibited a lower k_La than those running with lower viscosity mediums [12,13]. The presence of antifoam promoted bubble coalescence and therefore reduced k_La [13,14]. Apart from the liquid properties, the reactor design parameters such as the height of the column and the ratio between riser and downcomer cross-sectional area (A_d/A_r) could also affect the flow pattern and bubble size distribution in the airlift system.

The gas–liquid mass transfer is commonly considered as a function of bubble sizes, and is explicitly described in several empirical correlations such as Frossling's equation and Higbie's theory for bubble columns [15]. Although the application of airlift could be in mediums with various properties, most investigations on bubble size distribution are often confined to the system operated with water–air as liquid and gas phases, respectively. Salinity is known to alter the properties of water, for instance, it decreases the surface tension of the solution, and this could significantly affect the bubble size distribution. This, in turn, has notable influence on the gas–liquid mass transfer. This work therefore focused on the quantitative analysis of the influence of salinity on the hydrodynamics and mass transfer behavior of the annulus sparged internal loop airlift contactor.

2. Experimental

2.1. Apparatus

Experiments were carried out in an acrylic transparent airlift contactor as detailed in Fig. 1. The column was 1.2 m in height with an inside diameter of 0.137 m. The column was equipped with pressure taps along the contactor height for the measurement of pressure drop, ΔP, which was used to determine riser gas holdup, $\varepsilon_{g,r}$. A 1 m draft tube height was installed centrally in the column with a bottom clearance of 5 cm for liquid circulation. The ratio between cross-sectional areas of downcomer and riser (A_d/A_r) was altered by changing the draft tube diameter as provided in Table 1. Saline water was added into the column until the anaerated liquid height was 3 cm above the draft tube. The aeration was accomplished through a perforated ring sparger with 30 holes (1 mm in diameter) provided at the base of the annulus section. The sparger was made from PVC tubing with of 0.8 cm diameter. Air flow rate was controlled by a calibrated rotameter to give a range of superficial gas velocities, u_{sg}, from 0.01 to 0.07 m/s.

Table 1 summarizes detail of the operation of this system. The salinity was measured by OPTIK Handheld Refractometer and was controlled at 15, 30, and 45 ppt. The density of the solution was measured by pycnometer (UL/Y ADAPTER, MIDDLE BORO, MA 02346, U.S.A., Brook field ENGINEERING LABS INC.) at 100 rpm, 26.5 °C, and the surface tension was measured with KRUSS K10T (Du Noüy Ring). These properties were summarized in Table 2.

Table 1
Dimensions of draft tubes

Draft tube	Symbol	D_i (cm)	D_{io} (cm)	A_d/A_r (−)
1	ALC1	3.4	4	0.067
2	ALC2	7.4	8	0.443
3	ALC3	8.4	9	0.661
4	ALC4	9.4	10	1.008

Please cite this article in press as: D. Ruen-ngam, et al., Influence of salinity on bubble size distribution and gas–liquid mass transfer in airlift contactors, Chem. Eng. J. (2008), doi:10.1016/j.cej.2007.12.024

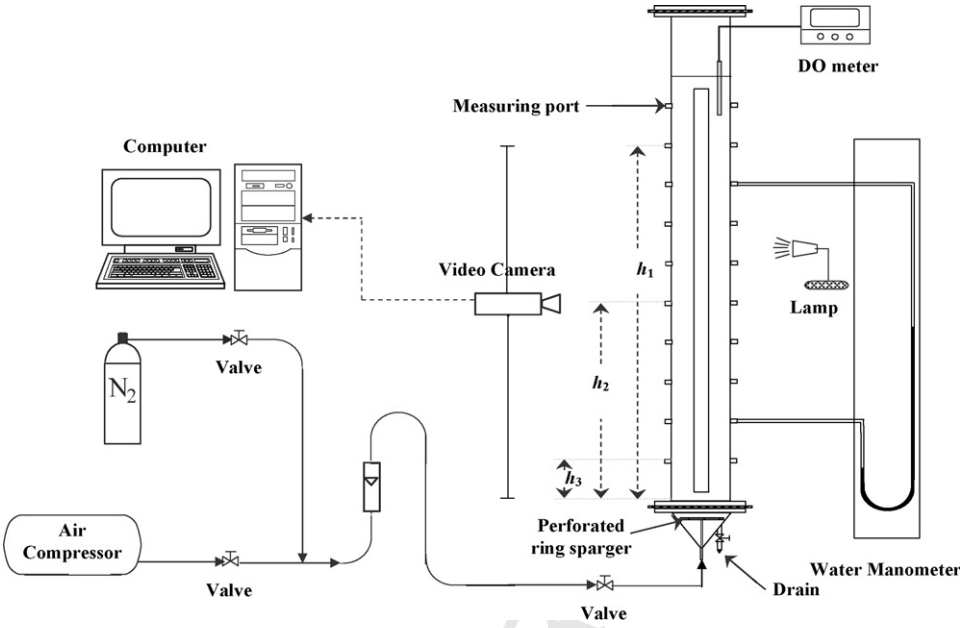

Fig. 1. Schematic diagram of concentric internal loop airlift contactor employed in this work.

Table 2
Liquid properties

Liquid phase	Surface tension (N/m)	Viscosity (kg/m s)	Density (kg/m^3)
Tap water	72.6×10^{-3}	1.28×10^{-3}	0.996×10^3
Sea water at 15 ppt	73.1×10^{-3}	1.44×10^{-3}	1.005×10^3
Sea water at 30 ppt	73.7×10^{-3}	1.47×10^{-3}	1.016×10^3
Sea water at 45 ppt	73.9×10^{-3}	1.49×10^{-3}	1.027×10^3

Table 3
Locations of digital video camera for bubble size measurement

Section	Height from the bottom end of the draft tube (h_i) (cm)
Top section (h_1)	90
Middle section (h_2)	50
Bottom section (h_3)	10

2.2. Bubble size distribution measurement

The bubble size measurement was performed in riser section using a photographic technique. More than 200 bubbles were photographed using a digital camcorder (Panasonic® NV-GS75) at three different heights (h_i): 10 cm (bottom section), 50 cm (middle section) and 90 cm (top section) from the base of the draft tube as illustrated in Fig. 1 and Table 3. The correction to real size was based on the scale attached to the draft tube with the same focal distance as the measured bubbles. The focus was adjusted on the scale and only the well-focalized bubbles were measured [4]. For ellipsoidal bubbles, the major and minor axes of bubble images were measured. The equivalent size of the bubble (d_B), representing the diameter of a sphere whose volume was equal to that of the bubble, is calculated using Eq. (1) [16,17] (Table 4).

$$d_B = (p^2 q)^{1/3} \quad (1)$$

2.3. Determination of hydrodynamic and mass transfer behavior of airlift contactors

The overall gas holdup, $\varepsilon_{g,o}$, was determined by the volume expansion method where:

$$\varepsilon_{g,o} = \frac{H_D - H_L}{H_D} \quad (2)$$

Table 4
Operating conditions for each ALC system

ALCs	Superficial gas velocity (m/s)					
	①	②	③	④	⑤	⑥
ALC1	0.008	0.012	0.018	0.022	0.030	0.035
ALC2	0.011	0.016	0.025	0.031	0.041	0.048
ALC3	0.013	0.019	0.029	0.036	0.048	0.056
ALC4	0.016	0.023	0.035	0.044	0.058	0.068
Symbol	·····	———	– – – –	-------	———	–·–·–

Please cite this article in press as: D. Ruen-ngam, et al., Influence of salinity on bubble size distribution and gas–liquid mass transfer in airlift contactors, Chem. Eng. J. (2008), doi:10.1016/j.cej.2007.12.024

The riser gas holdup, $\varepsilon_{g,r}$, was estimated by measuring the pressure difference (ΔP_m) between two pressure taps located along the height of the column (Δh) where:

$$\varepsilon_{g,r} = 1 - \frac{\Delta P_m}{\rho_l g \Delta h} \quad (3)$$

It was assumed that gas holdup in the top section was approximately equal to that in the riser and therefore the downcomer gas holdup, $\varepsilon_{g,d}$, could be computed from:

$$\varepsilon_{g,d} = \frac{\varepsilon_{g,o} H_D (A_d + A_r) + (H_{df} A_d - H_D (A_d + A_r))\varepsilon_{g,r}}{H_{df} A_d} \quad (4)$$

Liquid velocities both in riser and downcomer were measured using the color tracer technique. The pressure taps were employed as injection points of the color tracer and the recorded time of color tracer between the two points in the contactor was measured for the calculation of liquid velocity.

The overall volumetric mass transfer coefficient ($k_L a$) was determined by the dynamic method [18–20]. A dissolved oxygen meter (Jenway 9300) was used to record the changes in oxygen concentration with time in the ALC. The system was initially freed of O_2 by bubbling N_2 through the liquid for approx. 10 min. The calculation of $k_L a$ follows Eq. (5):

$$\ln \frac{(c* - c_\circ)}{(c* - c_L)} = k_L a t \quad (5)$$

3. Results and discussion

3.1. Local bubble size distribution in airlift systems

Fig. 2 illustrates examples of the bubble size distribution curves obtained from the various sections of the ALC system operated with saline water at 30 ppt and with $A_d/A_r = 0.661$. As a general trend, bubble size was quite large, in the range of 6.0–8.2 mm, at low superficial velocity. At higher gas throughput, bubbles became smaller in size and the distribution of bubble size became bimodal where there were two main bubble sizes present at the same time (2 and 6.5 mm). At high gas throughput, bubble size became small and the distribution illustrated that there was only one main bubble size in the system at this condition (2 mm). Bubble size did not seem to be smaller when the superficial velocity became higher than 0.036 m/s. This finding was for the system operated with water at salinity of 30 ppt, and it agreed well with the report by Wongsuchoto et al. [4] who carried out the experiment in fresh water systems that, at adequately high aeration, bubble no longer changed its size distribution ($u_{sg} > 0.05$ m/s). The difference was that the airlift operated with saline solution had smaller bubble sizes than those with fresh water.

3.2. Axial bubble size distribution in airlift contactors

The axial bubble size distribution was obtained by taking photographs of bubbles in the airlift at different heights. Bubble distribution frequency was then formulated for each sampling point, and the results are given in Fig. 2. In the top and middle

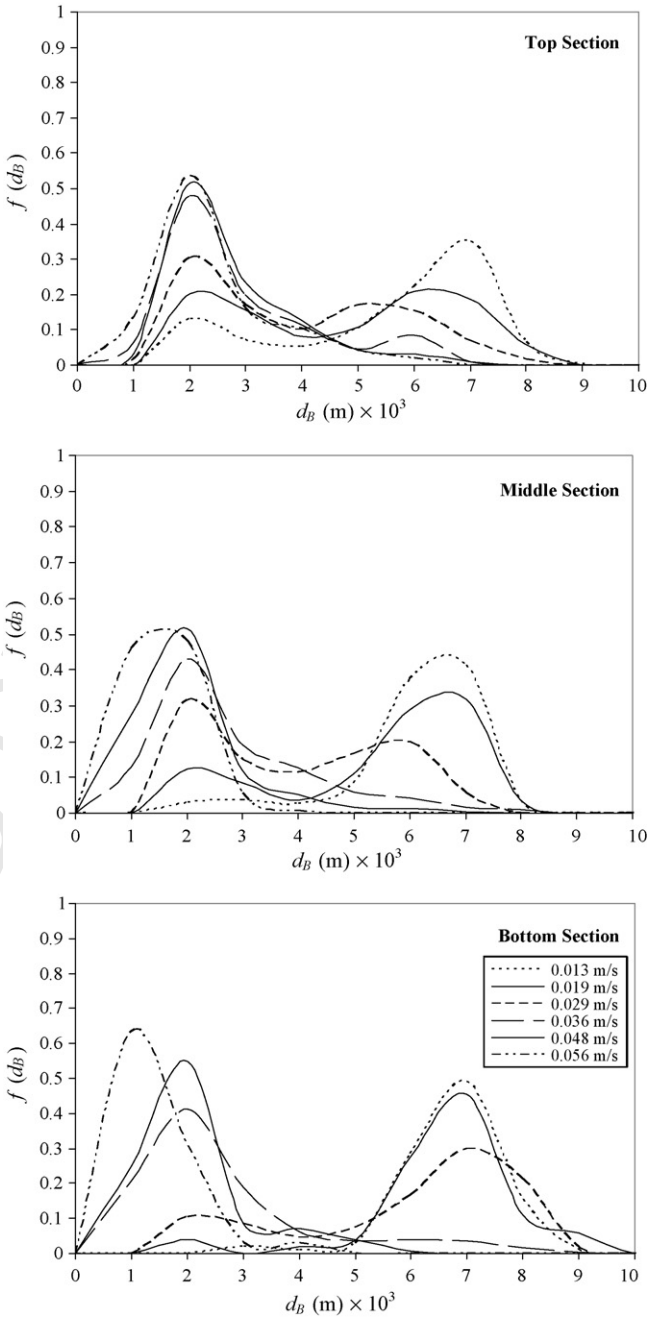

Fig. 2. Frequency distribution of bubble sizes at various superficial gas velocities in ALC with $A_d/A_r = 0.661$ (salinity = 30 ppt).

sections, the distribution changed from uni-modal to multi-modal curve at $u_{sg} \approx 0.019$ m/s whereas the bottom section saw this change at $u_{sg} \approx 0.029$ m/s. The breakage of the bubbles at high gas throughput was caused by higher amount of energy dissipation and turbulent which promoted more interaction between bubbles. The results suggested, therefore, that there was a higher level of turbulence in the top and middle sections than that in the bottom. Fig. 3 illustrates the mean values of the bubble sizes with the highest occurrence frequencies (Fig. 3(a)) compared with the average, Sauter mean diameter of bubbles (Fig. 3(b)) in the three sections in the airlift system with A_d/A_r of 0.661. This revealed that bubble size in the bottom section was slightly larger

Please cite this article in press as: D. Ruen-ngam, et al., Influence of salinity on bubble size distribution and gas–liquid mass transfer in airlift contactors, Chem. Eng. J. (2008), doi:10.1016/j.cej.2007.12.024

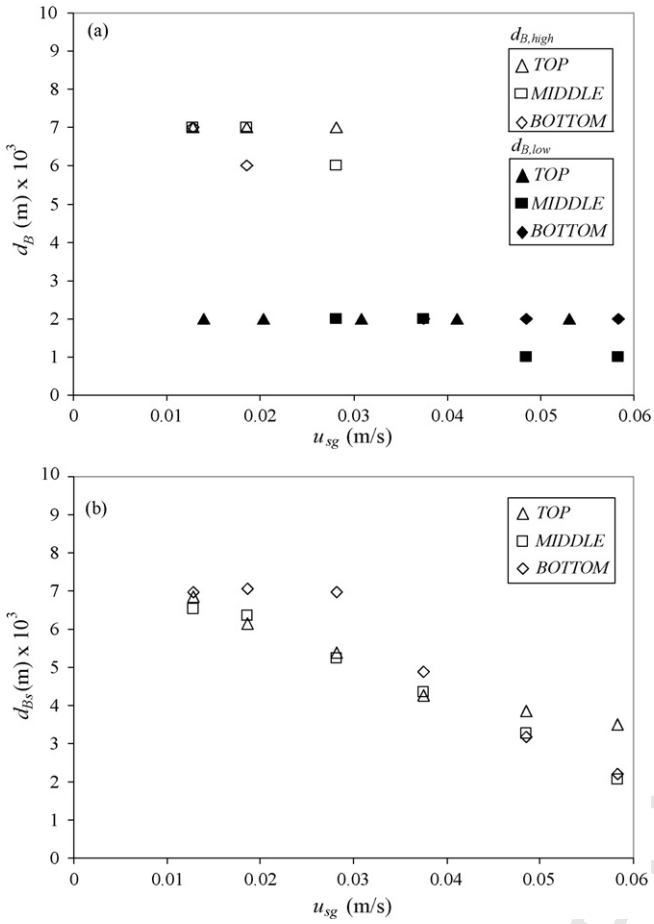

Fig. 3. Axial variation in bubble size in ALC with $A_d/A_r = 0.661$ (salinity = 30 ppt): (a) the average high bubble size ($d_{b,high}$) and average low bubble size ($d_{b,low}$), and (b) Sauter mean diameter.

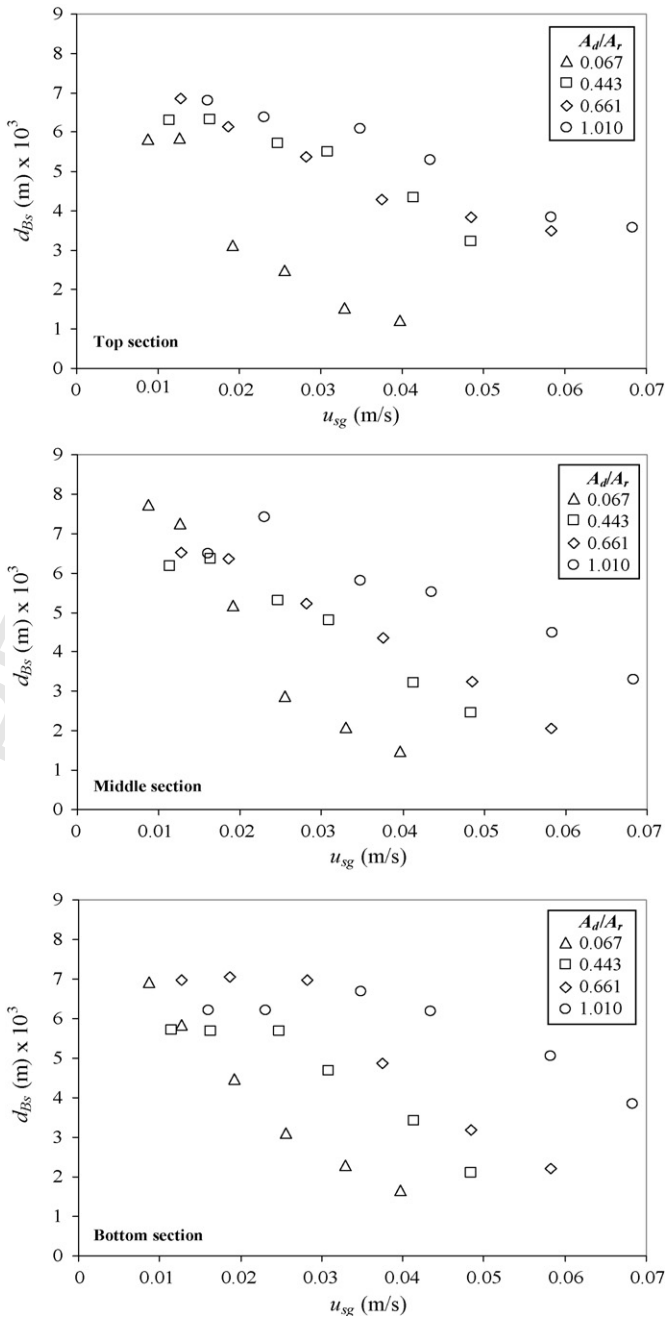

Fig. 4. Bubble sizes in ALC with different downcomer to riser cross-sectional area ratios (salinity = 30 ppt).

than in those in the other sections, particularly at a lower range of u_{sg} (<0.04 m/s) examined in this work. At a higher u_{sg} range, the effect of column height on the bubble size was not obvious and the sizes of bubbles were approximately the same throughout the length of the airlift. The same finding was found for the system running with tap water as described in Wongsuchoto et al. [4].

3.3. Effect of the ratio between downcomer and riser cross-sectional areas on bubble size

To investigate the effect of the ratio between the downcomer and riser cross-sectional areas (A_d/A_r), the experiment was conducted in the airlift contactors running with sea water at 30 ppt with four different draft tube sizes as detailed in Table 1 and the average bubble sizes are shown in Fig. 4. At a low range of u_{sg} (<0.015 m/s), no significant differences in bubble size were observed in all systems. At u_{sg} greater than 0.015 m/s, the differentiation of the bubble sizes in the systems with different draft tube sizes became more obvious, i.e. the bubble size was larger in the system with larger draft tube size (d_{Bs}, ALC4 > 3 > 2 > 1). In other words, the bubble size was larger in the system with smaller riser cross-sectional area. It was possible that turbulence in the system with smaller riser was stronger than those with larger riser, and increasing the chance of bubbles being coalesced. Fig. 4 also illustrates that the effect of A_d/A_r on bubble size was more obvious at the bottom section, and not as much in the middle and top sections. As stated earlier, the level of turbulence in the middle and top sections of the airlift was believed to be stronger than that in the bottom section. However, bubble sizes in this top section were not significantly regulated by A_d/A_r suggesting that, within the range of aeration employed in this work, similar level of turbulent intensity was resulted. On the other hand, the bottom section in the airlift with different A_d/A_r might be exposed to noticeable levels of turbulence inten-

Please cite this article in press as: D. Ruen-ngam, et al., Influence of salinity on bubble size distribution and gas–liquid mass transfer in airlift contactors, Chem. Eng. J. (2008), doi:10.1016/j.cej.2007.12.024

sities. This therefore resulted in a distinguishable bubble sizes as observed in Fig. 4.

3.4. Effect of salinity on average bubble size

Fig. 5(a–b) displays the relationship between bubble sizes in the ALC operated with saline water at different salinity levels. This figure illustrates that, at low range of u_{sg} (<0.02 m/s), the effect of salinity on bubble size was not obvious and bubble sizes were in the range of 6.0–7.5 mm in all ALC systems. At higher u_{sg}, the effect of salinity on bubble size became more apparent where the bubble size appeared to be smaller in the saline solution than that in fresh water. This was in contrast with the fact that saline solution possesses stronger surface tension and viscosity than water and the bubble size in such solution should be larger than that in water. However, in this case, the effect of electrolyte on viscosity (Marangoni effect) was reported not to be adequate to regulate the bubble size [21,22], and therefore the effects of salinity on bubble size were mainly due to its ionic properties. This finding was in good agreement with several past reports which stated that electrolyte solutions inhibited bubble coalescence and retarded bubble riser velocity which then reduced the bubble size [20,22–26]. It should be noted that types and concentration of electrolytes can impose different effects on bubble coalescence, for instance, Lessard and Zieminiski [20] ordered the coalescence efficiency in various electrolytes as follows: $MgSO_4 < MgCl_2 < CaCl_2 < Na_2SO_4 < LiCl < NaCl < NaBr < KCl$.

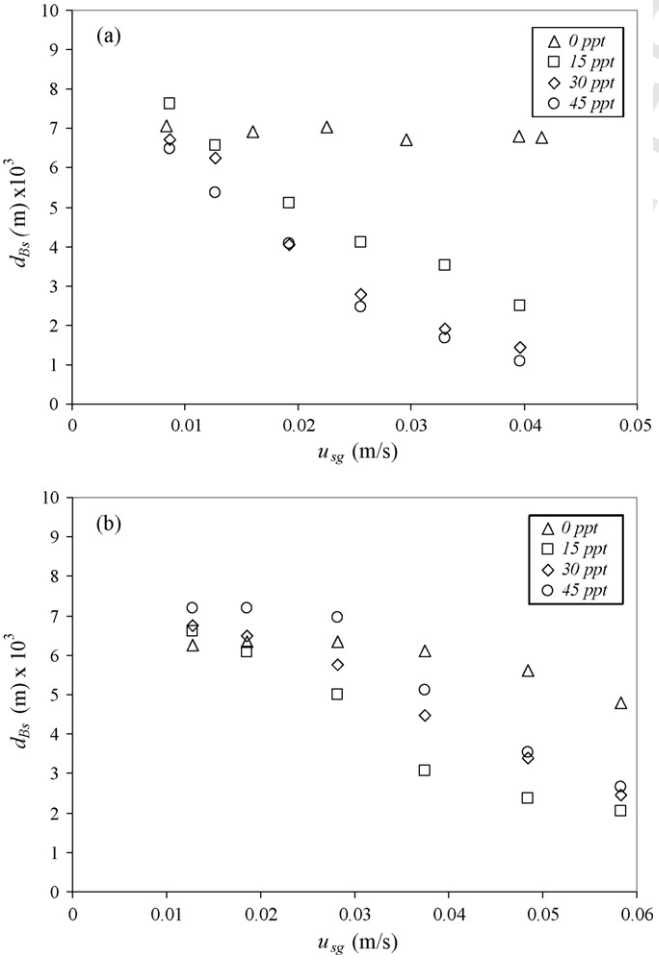

Fig. 5. Bubble sizes in ALC: (a) $A_d/A_r = 0.067$ and (b) $A_d/A_r = 0.661$.

Fundamentally, there are two types of forces or pressures dealing with the coalescence or breakup of the bubbles. The first one is the Laplace pressure which promotes bubble coalescence caused by the drainage of the liquid film located in between the two adjacent bubbles. This pressure depends on the reciprocal of the bubble diameter. However, if the Laplace pressure is too strong, bubbles coalesce very rapidly and this reduces the stability of the bubbles. Therefore, at this condition, bubble breakage dominates in the system. The other type of force is repulsive force. Electrolytes such as salt increased the repulsive hydration force by enhancing water structure due to hydrogen bond at the interface leading to a more stable bubble than that in the fresh water system. This formation of repulsive force balances the Laplace pressure, inhibiting bubble coalescence. The two forces can be written in a mathematical form as follows [27]:

$$\Delta P = \frac{\sigma}{r_p} - \Pi \tag{6}$$

when σ is surface tension, r_p is radius of intersection of three films called the Plateau border channel and the ratio between the surface tension and radius of intersection or (σ/r_p) is equal to Laplace pressure. Π is the repulsive pressure or disjoining pressure which is the summation of various forces between ions interaction at the gas and liquid interface according to Eq. (7).

$$\Pi = \Pi_{vdw} + \Pi_{DL} + \Pi_{hyd} \tag{7}$$

where Π_{vdw} is attractive van der Waals force, Π_{DL} is the dielectric double layer force or repulsive force and Π_{hyd} is short-range repulsive or hydration force. An attractive van der Waals force (Π_{vdw}) is a weak attraction force and caused from the polarization of molecules into dipoles, and can be expressed mathematically as in Eq. (8). A dielectric double layer (Π_{DL}) is the repulsive force caused from confinement of the ion charge at gas–liquid interface. A hydration forces was short-range repulsive force (Π_{hyd}) resulting from the formation of the water molecules near charged surfaces as in Eq. (9),

$$\Pi_{vdw} = \frac{-A}{6\pi h^3} \tag{8}$$

$$\Pi_{hyd} = \left(\frac{W}{\lambda}\right) \exp(-h/\lambda) \tag{9}$$

where A is the Hamaker constant which is equal to 10^{-20} J, h the film rapture thickness, λ the decay length of the hydration interaction, mostly takes the value of about 8.5 nm, and W the pre-exponential constant ≈6 mN/m^2 [27]. The film rapture thickness or h was reported to be a function of salinity by Cain and Lee [28] which were equal to 114.7, 106.8, 98.8, and 90.9 for the water with salinity levels of 0, 15, 30, and 45 ppt, respectively. In the same work [28], it was reported that the dielectric double layer force (Π_{DL}) was negligible compared with the hydration force and should be omitted from the calculation. Moreover, van der Waals attraction was generally reported to be relatively

Table 5
Estimates of disjoining pressures (Π) at different salinity levels

Salinity (ppt)	h[a] (nm)	van der Waals attraction (N/m^2)	Electrostatic repulsion (N/m^2)	Hydration repulsion (N/m^2)	Total pressure (Π) (N/m^2)
0	114.7	−0.35	0	0.97	0.62
15	106.8	−0.44	0	2.47	2.03
30	98.8	−0.55	0	6.29	5.74
45	90.9	−0.71	0	16.01	15.30

[a] [28].

small and was also negligible compared with the hydration force [21,22]. Therefore, Eq. (6) is reduced to

$$\Delta P = \frac{\sigma}{r_p} - \Pi_{hyd} \quad (10)$$

The pressure difference, ΔP, in Eq. (10) was important in controlling the level of bubble coalescence or bubble breakage in the system. ΔP is low for the condition with inhibiting bubble coalescence, and high for the bubble coalescence promoting conditions. Nevertheless, as mentioned above, a much higher ΔP would result in a breakup of bubbles [29]. A summary of these forces acting on the bubbles in the airlift systems is given in Table 5.

Let us define the parameter ΔP_C which is the level of ΔP below which the inhibition of bubble coalescence occurred, and above which bubble breakage prevailed. Therefore, the bubble had its greatest size at ΔP_C. Fig. 6 shows the summary of the various forces acting in the various saline solutions. As stated earlier, the bubble size in the water system was the largest and under this condition, ΔP in water was approx. 20 N/m^2 for the whole range of u_{sg} employed in this work as detailed in Table 6. This was due to the absence of repulsive force to balance the Laplace pressure. With the presence of salinity, the repulsive force became stronger. However, this repulsive force was not strong enough to bring ΔP down. In contrast, the Laplace pressure in the presence of salinity seemed to be quite large which could be the result from the increasing surface tension. This resulted in ΔP having a value greater than 20 N/m^2. Therefore, bubbles tended to break in such condition.

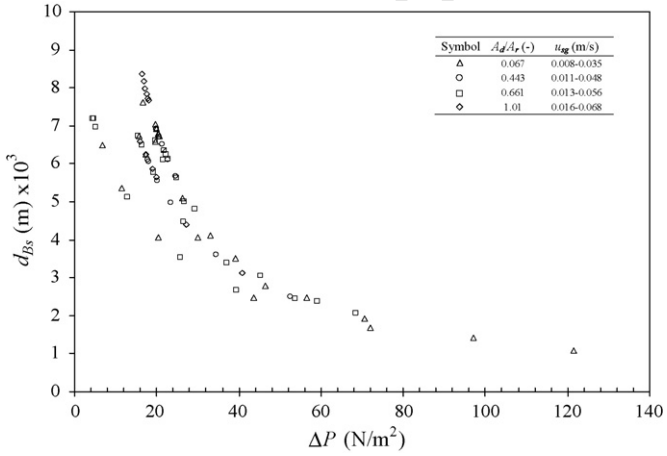

Fig. 6. Relationship between bubble size and ΔP.

In the airlift with A_d/A_r of 0.067 running with 45 ppt salinity, ΔP was about 43–121 N/m^2 at $u_{sg} > 0.02$ m/s and therefore bubble breakup was expected. The bubble size in this case was quite small, at 0.001–0.002 m (see Fig. 5(a)). Fig. 5(b) illustrates that when the A_d/A_r was altered (from 0.067 to 0.661), the condition in the system changed, and despite using the same level of u_{sg}, the system running with 45 ppt salinity had ΔP of 5–25 N/m^2 which prevented bubble breakup, therefore accommodating larger bubbles (0.005–0.006 m) than those in the airlift with lower A_d/A_r.

Fig. 6 illustrates the relationship between pressure driving forces and the average bubble size in all airlift systems employed in this work. It seemed that ΔP that gave the largest bubble size (ΔP_C) was in the range from 15 to 20 N/m^2.

3.5. Effect of superficial velocity

Fig. 5(a–b) demonstrates that Sauter mean diameter of the bubbles decreased with superficial gas velocity at all salinity levels. This finding agreed well with the reported data in the air-

Table 6
Estimates of pressure driving forces for average bubble size in different salinity levels in ALC with $A_d/A_r = 0.067$

Salinity (ppt)	u_{sg} (m/s)	ΔP (N/m^2)	d_{Bs} (m) × 10^3
0	0.008	19.61	7.05
	0.012	19.97	6.94
	0.018	19.62	7.05
	0.022	20.62	6.72
	0.030	20.36	6.81
	0.035	20.45	6.78
15	0.008	16.69	7.63
	0.012	19.76	6.58
	0.018	26.24	5.09
	0.022	33.10	4.11
	0.030	39.15	3.51
	0.035	56.48	2.48
30	0.008	15.61	6.73
	0.012	17.29	6.25
	0.018	30.00	4.06
	0.022	46.38	2.80
	0.030	70.66	1.92
	0.035	97.02	1.43
45	0.008	6.79	6.48
	0.012	11.54	5.37
	0.018	20.30	4.07
	0.022	43.73	2.47
	0.030	71.90	1.68
	0.035	121.4	1.08

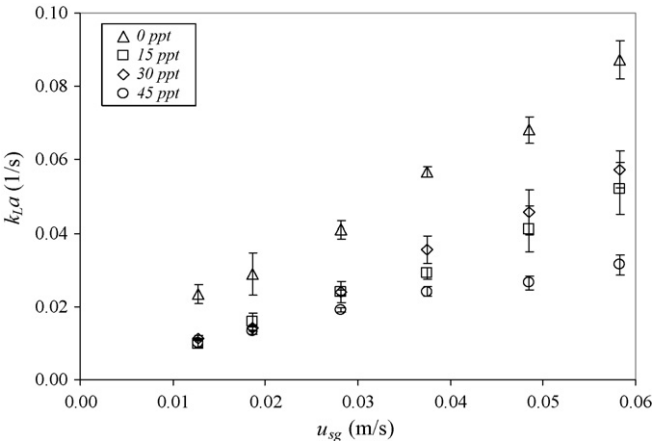

Fig. 7. Overall volumetric mass transfer coefficient (ALC with $A_d/A_r = 0.661$).

lift systems operated with various types of liquid [2–4,30]. The bubble sizes were regulated by the level of pressure difference in the airlift system as described earlier. At low range of gas flow rate (<0.02 m/s) as shown in Fig. 5(a), the pressure difference was in the range of 15–20 N/m^2, and this enhanced bubble size. At a higher range of superficial gas velocity (>0.02 m/s), ΔP was higher than 20 N/m^2 which promoted the breakup of the bubbles. In addition, at this high gas throughput conditions, the airlift contained a relatively high gas holdup which also enhanced the chance of bubbles collision and breaking up.

3.6. Overall volumetric mass transfer coefficient (k_La) in the airlift systems operating with sea water

The overall volumetric mass transfer coefficient (k_La) was calculated from Eq. (5). The change in k_La with u_{sg} and salinity level is illustrated in Fig. 7 which shows that k_La increased with superficial gas velocity but decreased with an increase in salinity. Salinity seemed to have adverse effects on k_La and the system with fresh water always imposed a higher k_La than those running with sea water. In addition, the effect of salinity on k_La was quite complicated. At low range of u_{sg} (<0.03 m/s), the effect of salinity did not seem to be significant, however, the effect became more pronounced at high aeration rate ($u_{sg} > 0.03$ m/s) and k_La was the highest at 30 ppt followed by those at 15 and 45 ppt, respectively.

This k_La quantity composed two main parameters, i.e. "k_L" or overall mass transfer coefficient, and "a" or specific interfacial area. Generally k_L was reported to be a function of turbulence, liquid properties and bubble size. The specific interfacial area (a) can be estimated using Eq. (11):

$$a = \frac{6\varepsilon_g}{d_{Bs}(1-\varepsilon_g)} \tag{11}$$

where $\varepsilon_{g,r}$ is the riser gas holdup and d_{Bs} Sauter mean diameter which is defined as:

$$d_{Bs} = \frac{\sum n_i d_{B,i}^3}{\sum n_i d_{B,i}^2} \tag{12}$$

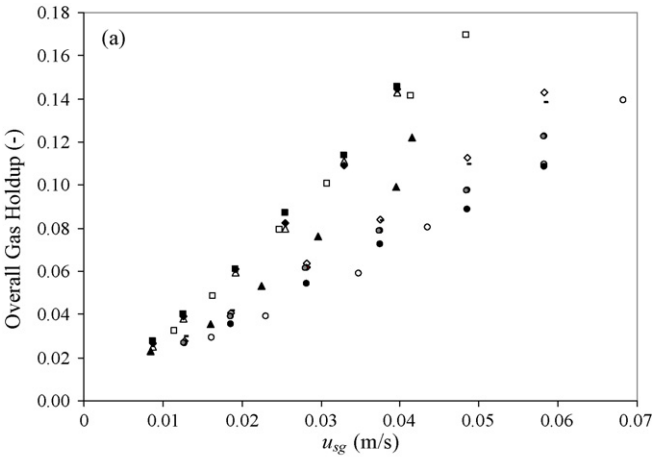

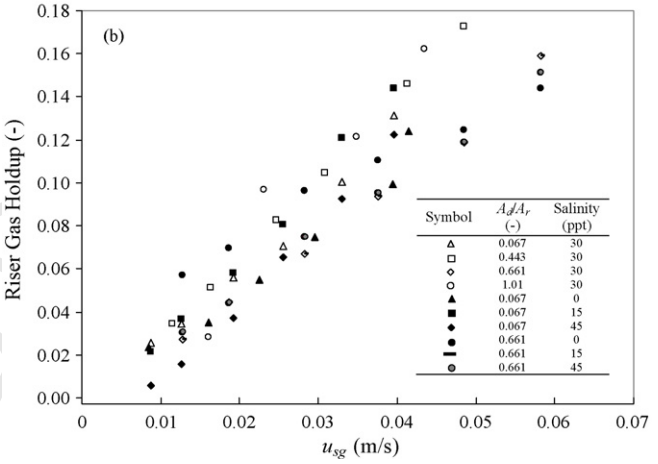

Fig. 8. Effects of superficial gas velocity, u_{sg}, on gas holdups.

where n_i is the occurrence frequency number of the sphere bubbles diameter, $d_{B,i}$. The two parameters significant for the determination of the specific mass transfer area were average bubble size (Fig. 5(b)) and gas holdup. Fig. 8 illustrates that the effect of salinity on gas holdups in the system was only marginal and the specific area should only vary with bubble size. As discussed earlier, the bubble size in sea water was smaller than that in fresh water and became smaller with an increase in superficial gas velocity. Therefore, the specific interfacial areas obtained in the systems at all salinity levels were higher than that in the fresh water system.

It was primarily assumed that the gas holdup was uniform throughout, both in axial and radial directions. The estimates of specific interfacial area (a) in the airlift system with $A_d/A_r = 0.661$ at various salinities is displayed in Fig. 9. This finding revealed that effect of salinity on specific area was only marginal at low range of superficial gas velocity ($u_{sg} < 0.028$ m/s), and became more significant at higher u_{sg}. The largest gas–liquid surface area was obtained from the airlift operating with saline water at 15 ppt, followed by those at 30 and 45 ppt. This corresponded well with the information on the effect of salinity on bubble size in Fig. 5(b).

Now that the information on k_La and a became known, the overall mass transfer coefficient or k_L could simply be calculated

Please cite this article in press as: D. Ruen-ngam, et al., Influence of salinity on bubble size distribution and gas–liquid mass transfer in airlift contactors, Chem. Eng. J. (2008), doi:10.1016/j.cej.2007.12.024

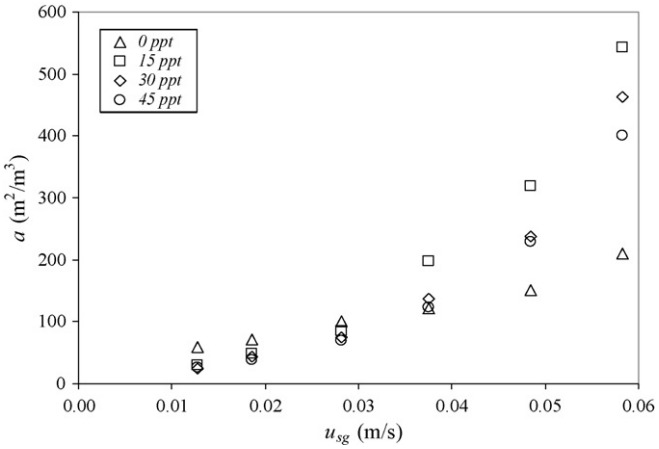

Fig. 9. Specific interfacial area in ALC ($A_d/A_r = 0.661$).

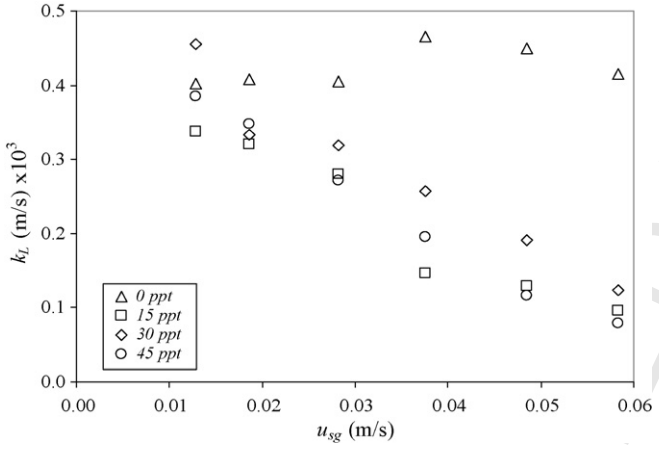

Fig. 10. Effects of superficial gas velocity, u_{sg}, on overall specific mass transfer coefficient, k_L, in ALC ($A_d/A_r = 0.661$).

by dividing k_La with a and the results are given in Fig. 10. The results revealed that k_L only became significantly different at high u_{sg}. The pure water system provides the highest level of k_L. Among the saline solutions, k_L was highest in the system with salinity of 30 ppt, followed by that with 45 ppt and 15 ppt, respectively. The reason fore this variation still could not be retrieved from this experiment. However, it was observed that the trend in k_La followed that of k_L quite closely, i.e. the highest was in pure water system, followed by those in saline concentrations of 30, 45 and 15 ppt, respectively.

3.7. Estimate of k_La

The mass transfer rate for the entire contactor was proposed in the terms of the overall volumetric mass transfer coefficient $(k_La)_T$ and could be calculated from sum of the mass transfer rates in riser and downcomer section as follows:

$$(k_La)_T = \frac{(k_La)_r V_{L,r} + (k_La)_d V_{L,d}}{V_{L,T}} \quad (13)$$

where $V_{L,r}$ is the volume of liquid in riser, $V_{L,d}$ the volume of liquid in downcomer and $V_{L,T}$ the volume of total liquid. $(k_La_L)_r$ and $(k_La_L)_d$ were then obtained from multiplied $k_{L,r}$ by $a_{L,r}$ and $k_{L,d}$ by $a_{L,d}$.

As a was obtained from the measurement, the estimate of k_La requires only the estimation of k_L. As mentioned above, the mass transfer coefficient, k_L was reported as a function of liquid properties and bubble size. It was assumed that Schmidt number remained constant as salinity did not significantly alter the properties of the liquid [15,31–33], and hence, the dimensionless relationship between Sherwood number (Sh), Reynold number (Re), Schmidt number (Sc) and Grashof number (Gr) could be formulated as follows:

forced convection

$$Sh = a + b Gr^c Sc^d + e\, Re^f\, Sc^h \quad (14)$$

free convection

Generally, Grashof number, Gr, represents the mass transfer by natural convection or free rise velocity whilst Reynolds number, Re, is the mass transfer form forced convection:

$$Gr = \frac{d_{Bs}^3 \rho_l \Delta\rho g}{\mu_l^2} \quad (15)$$

$$Re = \frac{d_{Bs} v_s \rho_l}{\mu_l} \quad (16)$$

The velocity and bubble diameter used in the calculation of Reynolds number were the slip velocity, v_s, and Sauter mean diameter, d_{Bs}. The slip velocity in riser, $v_{s,r}$ was calculated as a function of the terminal rise velocity of a single bubble, u_∞, which were related to hindering effects from neighboring bubbles in the riser section. Information on bubble sizes was then employed to estimate the slip velocity of the gas bubbles in the system using the following equation [34,35]:

$$v_{s,r} = \frac{u_\infty}{(1 - \varepsilon_{g,r})} \quad (17)$$

where u_∞ is the terminal bubble riser velocity which can be calculated using the correlation proposed by Jamialahmadi et al. [36].

$$u_\infty = \frac{(1/8)((\rho_l - \rho_g)/\mu_l) g d_{Bs}^2 ((3\mu_l + 3\mu_g)/(2\mu_l + 3\mu_g)) \sqrt{2\sigma/d_{Bs}(\rho_l + \rho_g) + g d_{Bs}/2}}{\sqrt{[(1/8)((\rho_l - \rho_g)/\mu_l) g d_{Bs}^2 ((3\mu_l + 3\mu_g)/(2\mu_l + 3\mu_g))]^2 + 2\sigma/d_{Bs}(\rho_l + \rho_g) + g d_{Bs}/2}} \quad (18)$$

The parameters a–h in Eq. (14) was then determined from experiments.

Eq. (14) must be used to predict $k_{L,r}$ and $k_{L,d}$, and in doing so, the slip velocities or terminal rise velocities in both riser and downcomer must be known (from Eqs. (17) and (18)) for the calculation of Reynolds number. As the photographic technique

Table 7
Parameter estimates for correlation in Eq. (14) $Sh = a + bGr^c Sc^d + eRe^f Sc^h$

Salinity (ppt)	Parameter							R^2
	a	b	c	d	e	f	h	
0	0.41	1.05	048	0	0	0	0	0.91
15–45	0.41	1.04	0.16	0.3	0.13	0.46	0.06	0.81
Q6 0 [4]	0.5	1.07	0.47	0	0	0	0	0.92

could only be used to measure the bubble size in riser, bubble size in downcomer was not known and the determination of slip velocity in downcomer was not possible. However, the average bubble size in downcomer ($d_{B,d}$) could be estimated from the downcomer liquid velocity, $u_{L,d}$, by assuming that the liquid must have velocity equaled to the terminal velocity to be able to drag the bubble down into the downcomer, or

$$v_{s,d} = u_{L,d} \tag{19}$$

Once the terminal velocity was known, the Levich equation [37] as shown in Eq. (19) was proposed for the calculation of bubble size:

$$d_{B,d} = \frac{1.8}{g}\left(\frac{u_{L,d}}{2}\right)^2 \tag{20}$$

Assume that there was no variation of bubble size along the radial and axial directions in downcomer:

$$d_{Bs,d} = d_{B,d} \tag{21}$$

The $a_{L,d}$ was calculated from substitution of $d_{Bs,d}$ from Eq. (21) and $\varepsilon_{g,d}$ from the experiment to Eq. (4).

The parameters a–h in Eq. (14) were evaluated using non-linear parameter fittings using all the results available in this work, and the results are given in Table 7 (noted that these parameters were obtained from the solver function in the MS Excel 97 where the objective was a minimal error between experimental and simulation data). For the case of tap water, the results from parameter fitting were reasonably close to those proposed from Wongsuchoto et al. [4] (as shown in the last row of Table 7). The fittings for the saline water gave somewhat different results from that for pure water in that the terms Reynolds number was not involved in the pure water system, but it was, to certain extent, for the saline water systems. This meant that the mechanism controlling the mass transfer coefficient in pure water was only the natural convection whereas the force convection as represented by the Reynolds term also was significant in the system operated with saline water. Fig. 11 illustrates the comparison between the calculated and experimental k_La of the airlift contactor operated with various saline solutions.

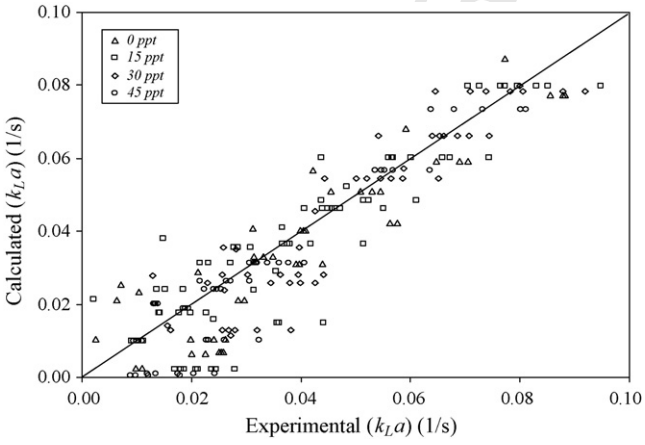

Q5 Fig. 11. Comparison of k_La from experiment and k_La estimated by Eq. (4.9) in ALC (A_d/A_r = 0.067–0.661).

4. Conclusion

This work continued our previous work on the bubble size distribution in the airlift systems. The distribution of bubble size in saline solution which was often used in cell cultivation was provided. Mechanisms for the bubble breakup/coalescence were proposed. The relationship between bubble size, liquid properties and the gas–liquid mass transfer behavior was investigated where the correlation for the estimate of the overall volumetric mass transfer coefficient was proposed with reasonable accuracy. This information will be useful in the future design of the airlift reactors for specific applications.

Acknowledgements

The authors wish to acknowledge the Thailand Research Fund and the Graduated Research Fund at Chulalongkorn University, THAILAND, for their financial supports.

References

[1] M.Y. Chisti, Airlift Bioreactors, Elsevier Applied Science, London/New York, 1989.
[2] D. Colella, D. Vinci, R. Bagatin, M. Masi, E.A. Bakr, A study on coalescence and breakage mechanisms in three different bubble columns, Chem. Eng. Sci. 54 (1999) 4767–4777.
[3] M. Polli, M.D. Stanislao, R. Bagatin, E.A. Bakr, M. Masi, Bubble size distribution in the sparger region of bubble columns, Chem. Eng. Sci. 57 (2002) 197–205.
[4] P. Wongsuchoto, T. Charinpanitkul, P. Pavasant, Bubble size distribution and gas–liquid mass transfer in airlift contactors, Chem. Eng. J. 92 (2003) 81–90.
[5] K. Kaewpintong, A. Shotipruk, S. Powtongsuk, P. Pavasant, Photoautotrophic high-density cultivation of *Haematococcus pluvialis* in airlift bioreactor, Bioresour. Technol. 98 (2007) 288–295.
[6] S. Krichnavaruk, W. Loataweesup, S. Powtongsook, P. Pavasant, Optimal growth conditions and the cultivation of *Chaetoceros calcitrans* in airlift photobioreactor, Chem. Eng. J. 10 (2005) 91–98.

[7] S. Krichnavaruk, S. Powtongsook, P. Pavasant, Enhanced productivity of *Chaetoceros calcitrans* in airlift photobioreactors, Bioresour. Technol. 98 (2007) 2123–2130.
[8] J. Bo, P. Lant, Flow regime, hydrodynamics, floc size distribution and sludge Properties in activated sludge bubble column, air-lift and aerated stirred reactors, Chem. Eng. Sci. 59 (2004) 2379–2388.
[9] N. Kantarci, F. Borak, O.K. Ulgen, Bubble column reactors, review, Process Biochem. 40 (2005) 2263–2283.
[10] M. Bouaifi, G. Hebrard, D. Bastoul, M. Roustan, A comparative study of gas holdup, bubble size, interfacial area and mass transfer coefficients in stirred gas–liquid reactors and bubble columns, Chem. Eng. Proc. 40 (2001) 97–111.
[11] J.C. Merchuk, A. Contreras, F. Garcia, E. Molina, Studies of mixing in a concentric tube airlift bioreactor with different spargers, Chem. Eng. Sci. 53 (1998) 709–719.
[12] L. Guo-Qing, Y. Shou-Zhi, C. Zhao-Ling, C. Jia-Yong, Mass transfer and gas–liquid circulation in an airlift bioreactor with viscous non-newtonian fluid, Chem. Eng. J. The Biochem. Eng. J. 56 (1995) B101–B107.
[13] J.M.T. Vasconcelos, J.M.L. Rodrigues, S.C.P. Orvalho, S.S. Alves, S.R.L. Mende, A. Reis, Effect of contaminants on mass transfer coefficients in bubble column and airlift contactors, Chem. Eng. Sci. 58 (2003) 1431–1440.
[14] W.A. Al-Masry, Effects of antifoam and scale-up on operation of bioreactors, Chem. Eng. Processing 38 (1999) 197–201.
[15] P. Painmanakul, K. Loubére, G. Hebrard, M. Mietton-Peuchot, M. Roustan, Effect of surfactants on liquid-side mass transfer coefficients, Chem. Eng. Sci. 60 (2005) 6480–6491.
[16] G. Hebrard, D. Bastoul, M. Roustan, Influence of the gas sparger on the hydrodynamic behavior of bubble columns, Trans. Inst. Chem. Eng. 74 (1996) 406–414.
[17] A. Couvert, M. Roustan, P. Chatellier, Two-phase hydrodynamic study of a rectangular airlift loop reactor with an internal baffle, Chem. Eng. Sci. 54 (1999) 5245–5252.
[18] M.Y. Chisti, M. Moo-Young, Hydrodynamics and oxygen mass transfer in a pneumatic bioreactor devices, Biotechnol. Bioeng. 31 (1988) 487–494.
[19] K. Koide, H. Sato, S. Iwamoto, Gas holdup and volumetric liquid-phase mass transfer coefficient in bubble column with draught tube and with gas dispersion into annulus, J. Chem. Eng. Jpn. 16 (5) (1983) 407–413.
[20] R.R. Lessard, A.S. Zieminiski, Bubble coalescence and gas transfer in aqueous electrolytic solutions, Ind. Eng. Chem. Fundam. 10 (1971) 260–269.
[21] G. Marrucci, A theory of coalescence, Chem. Eng. Sci. 24 (1969) 975–985.
[22] M.J. Prince, H.W. Blanch, Transition electrolyte concentrations for bubble coalescence, AIChE J. 36 (1990) 1425–1429.
[23] G. Marrucci, L. Nicodemo, Coalescence of gas bubbles in aqueous solution of inorganic electrolytes, Chem. Eng. Sci. 22 (1967) 1257–1265.
[24] M.J. Prince, H.W. Blanch, Bubble coalescence and breakup in air-sparged bubble column, AIChE J. 36 (1990) 1485–1499.
[25] P.K. Weissenborn, R.J. Pugh, Surface tension of aqueous solutions of electrolytes: relationship with ion hydration, oxygen solubility, and bubble coalescence, J. Colloid Interface Sci. 184 (1996) 550–563.
[26] K. Malysa, M. Krasowska, M. Krzan, Influence of surface active substances on bubble motion and collision with various interfaces, Adv. Colloid Interface Sci. 114–115 (2005) 205–225.
[27] Y.H. Tsang, K. Young-Ho, L.K. Donald, Bubble-size dependence of the critical electrolyte concentration for inhibition of coalescence, J. Colloid Interface Sci. 275 (2004) 290–297.
[28] W.F. Cain, C.J. Lee, A technique for studying the drainage and rupture of unstable liquid films formed between two captive bubbles, J. Colloid Interface Sci. 106 (1985) 70–85.
[29] S. Hartland, Surface and Interface Tension: Measurement, Theory, and Applications Basel:, Marcel Dekker, New York, 2004.
[30] A. Contreras, F. Garcia, E. Molina, J.C. Merchuk, Influence of sparger on energy dissipation, shear rate, and mass transfer to sea water in a concentric-tube airlift bioreactor, Enzyme Microb. Technol. 25 (1999) 820–830.
[31] R. Higbie, Rate of absorption of a pure gas into a still liquid during short period of exposure, Trans. Am. Inst. Chem. Eng. 31 (1935) 365–389.
[32] P.H. Calderbank, Mass transfer in fermentation equipment, in: N. Blakebrough (Ed.), Biochemical and Biological Engineering Science, vol. 2, Academic Press, New York, 1967.
[33] J.E. Bailey, D.F. Ollis, Biochemical Engineering Fundamentals, McGraw-Hill, New York, 1977.
[34] G. Marrucci, Rising velocity of a swarm of spherical bubbles, Ind. Eng. Chem. Fundam. 4 (1965) 224–225.
[35] G.B. Wallis, One Dimensional Two-Phase Flow, McGraw-Hill, New York, 1969.
[36] M. Jamialahmadi, C. Branch, Müller-Steinhagen, Terminal bubble rise velocity in liquid, Trans. Inst. Chem. Eng. Part A 72 (1994) 119–122.
[37] V.G. Levich, Physiochemical Hydrodynamis, Prentice-Hall, Englewood Cliffs, NJ, 1962.

Please cite this article in press as: D. Ruen-ngam, et al., Influence of salinity on bubble size distribution and gas–liquid mass transfer in airlift contactors, Chem. Eng. J. (2008), doi:10.1016/j.cej.2007.12.024